Fabrication of Copper Sulphide through Single Source Precursors for Photocatalytic and Battery Applications

A dissertation submitted to the Department of Chemistry, Quaid-i-Azam University, Islamabad, in partial fulfillment of requirements for the degree of

Master of Philosophy

in

Inorganic/Analytical Chemistry

by

UMAIR SHAMRAIZ

Department of Chemistry
Quaid-i-Azam University
Islamabad
2015

Fabrication of Copper Sulphide through Single Source Precursors for Photocatalytic and Battery Applications

By

UMAIR SHAMRAIZ

Department of Chemistry
Quaid-i-Azam University
Islamabad
2015

DECLARATION

This is to certify that this dissertation entitled "Fabrication of Copper Sulphide through Single Source Precursors for Photocatalytic and Battery Applications" submitted by Mr. Umair Shamraiz is accepted in its present form by the Department of Chemistry, Quaid-i-Azam University, Islamabad, Pakistan, as satisfying the partial fulfillment for the degree of M.Phil in Inorganic/ Analytical Chemistry.

External Examiner : _____

Supervisor: _____

Prof. Dr. Amin Badshah
Department of Chemistry
Quaid-i-Azam University
Islamabad.

Head of Section: _____

Prof. Dr. Syed Ahmad Tirmazi
Department of Chemistry
Quaid-i-Azam University
Islamabad.

Chairman: _____

Prof. Dr. Amin Badshah
Department of Chemistry
Quaid-i-Azam University
Islamabad.

IN THE NAME OF ALLAH, THE MOST GRACIOUS, THE MOST MERCIFUL

THEN WHICH OF THE FAVORS OF YOUR LORD WILL YOU DENY?

DEDICATED TO MY LOVING PARENTS

CONTENTS

Page

ACKNOWLEDGEMENT

First of all I am grateful to ALMIGHTY ALLAH and the Holy Prophet Muhammad (SAW), for every good thing which I have in my life.

My gratitude is for my supervisor Prof. Dr. Amin Badshah for his guidance, valuable suggestions and encouragements during my Mphil.

I am indebted to my father Shamraiz Khan and I am thankful to Almighty Allah that my mother prays for my success today and huge contribution in my achievements is because of her prayers. I am thankful to my family members my sisters and brothers.

I would like to extend my wholehearted thanks to Dr. S. A. Tirmazi (Head of Inorg/Ana Chemistry), and all my teachers from my nursery class to present time for their efforts and help.

A deep sense of gratitude to Dr. Raja Azadar Hussain for his keen interest during my research and his help at each and every step of my research work. I have no words to thank the hard work that he has done for me. He was always there to pull me out whenever I got stuck during my research and one more thing which I would like to mention is his moral support during my entire university career.

I have no words to thank the hard work of Dr. Imtiaz Nadeem for EDX, SAED, TEM and HRTEM and Dr. Shafiqullah Marwat for Battery applications.

I am thankful to all my lab fellows and friends for their support during my research work.

I am thankful to the technical staff at the Department of Chemistry, Quaid-i-Azam University Islamabad namely Tayyab, Irfan, Rana Matloob, Rana Tahir, Danish and Shareef Chuhan.

UMAIR SHAMRAIZ

Abstract

In the present work CuS nanoparticles have been successfully synthesized by using different novel copper thiourea complexes as a single source precursor. All of these have been characterized by PXRD, TEM, HRTEM, EDX and SAED. The CuS prepared with average of less than 30 nm has been confirmed. Photocatalytic activity is successfully performed under direct sunlight (outdoor lightening) against five different organic dyes which was monitored with the help of UV-visible spectroscopy. The results shows that synthesized nanoparticles are efficient photocatalyst. Except for methyl orange the degradation efficiency for all the dyes was achieved to be more than 80%. Battery applications are evaluated for 3NACuS by testing electrochemical discharge/charge at voltage limits of 1.8 −2.6 V versus Li/Li+.

Abbreviations

DTO	Dithiooximide
TAA	Thioacetamide
CVD	Chemical vapor deposition method
thd	Tetramethylheptanedionate
CVR	Chemical vapor reaction
BMIM	Butyl-3-methylimidazolium
HMA	Hexamethylinetetramine
NPs	Nanoparticles
di-HCF_4	Bis(2,2,3,3,4,4,5,5-octafluoro-1-pentyl)-2-sulfosuccinate
CuTU	Copper Thiourea
Glu	Glutamic acid
ISTIR	In situ source-template-interface reaction
en	Ethylene diamine
TEA	Triethanolamine
dtc	Dithiocarbamate
CD	Chemical deposition
PTA	Photothermal ablation
CNTs	Carbon nanotubes
OCV	Open circuit voltage
XRD	X-ray diffraction

PL	Photoluminiscent
eV	Electron Volt
MB,	Methylene blue
MG	Malachite green
RhB	Rhodamine B
MO	Methyl orange
MR	Methyl red
MV	Methyl violet
TEM	Transmission electron microscope
CTEM	Conventional transmission electron microscopic
SAED	Selected area electron diffraction
CCD	Charge coupled devices
TU1	1-(4-nitrophenyl)-3-propionylthiourea
TU2	1-(3-nitrophenyl)-3-propionylthiourea
TU3	1-(2-chloro-4-nitrophenyl)-3-propionylthiourea
TU4	1-(2-methoxy-4-nitrophenyl)-3-propionylthiourea
TU5	1-(2-methyl-4-nitrophenyl)-3-propionylthiourea
DCM	Dichloromethane

CuTU1	Bis(1-(4-nitrophenyl)-3-propionylthiourea)copper(II)
CuTU2	Bis(1-(3-nitrophenyl)-3-propionylthiourea)copper(I)
CuTU3	Bis(1-(2-chloro-4-nitrophenyl)-3-propionylthiourea)copper(II)
CuTU4	Bis(1-(2-methoxy-4-nitrophenyl)-3-propionylthiourea)copper(II)
CuTU5	Bis(1-(2-methyl-4-nitrophenyl)-3-propionylthiourea)copper(II)

CHAPTER 1

INTRODUCTION

1. Introduction to Copper Sulphide

Copper sulphide is a binary inorganic material which has a general formula Cu_xS_y. Both the synthetic materials and minerals contain CuS (covellite) and Cu_2S (chalcocite). Copper sulphide is one of the most important metal chalcogenides which has attracted much interest in the recent research due to its special properties and potential applications. Both CuS and Cu_2S exhibit metallic properties and transforms in to superconductor at about 1.6 K. In addition to superconductivity these materials also exhibit fast ion conduction at high temperature [1]. Due to small size CuS nanoparticles exhibit excellent, physical, chemical, structural and surface properties which are very much different from bulk material. In the last few decades the synthesis and characterization of CuS nanostructures have become an interesting area of research. It has been observed that the properties of this material are dependent on the morphologies such as nanowires, nanoplates, nanotubes, hollow spheres, nanorods, flowerlike structures, nanoribbons and complex hierarchal micro/nanostructures [2]. Covellite (CuS) has wide range applications in photocatalysis, solar cells, sensors and as a cathode material in lithium chargeable batteries etc. While chalcocite (Cu_2S) is a p-type semiconductor having a band gap of 1.21 eV which is in the range for solar energy conversion and it can be used in solar cells, photocatalysts, biosensors and optioelectronic devices [1].

CuS generally exists in hexagonal crystalline phase and provides the prominent peaks in PXRD at 2θ values 27.78, 29.36, 31.87 and 47.96 for 101, 102, 103 and 110 planes (Figure 1.1).

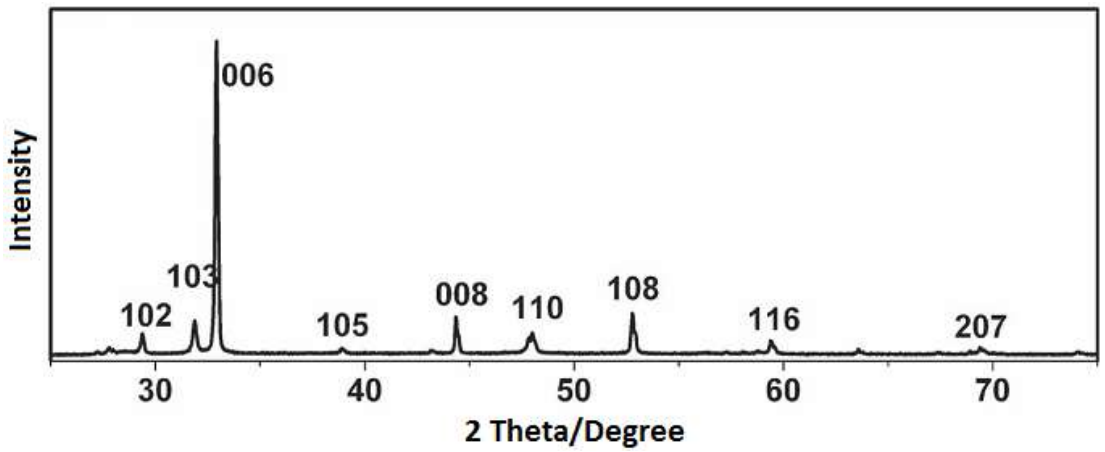

Figure 1.1 PXRD pattern of hexagonal CuS. Modified with permission of Qiwei Tians et al. Adv. Mater. 2011, 23. Copyright Willeyonline library.

It has now been established that copper sulphide is active spectroscopically (in UV-vis spectrum yields a peak at 620 nm) as well as electrochemically (during cyclic voltammetry provides couple of redox peaks between -0.4 V to -0.7 V in a reversible electrochemical process) [3].

Importance of CuS in semiconducting materials is because of its nonlinear optical properties [4], increased conductivity at high temperature [5], excellent solar radiation absorbing characteristics [6] and high capacity cathode material in lithium secondary batteries [7]. At low temperature copper sulphide acts as a metallic conductor and readily transforms into superconducting material at 1.6 K [8]. Copper sulphide with different morphologies has different band gaps e.g. CuS microspheres have band gap of 2.08 eV, CuS nanotubes have band gap of 2.06 eV, CuS nanoflakes have band gap of 2.16 eV and CuS nanoparticles have band gap of 1.88 eV. All these morphologies bear different absorbance edges both in UV and visible region. CuS nanostructures exhibits unique size dependent properties i.e. they bears efficient absorbance in visible region from 400 to 550 nm and a strong blue emission band at 465 nm makes it a good photo luminescent material. These properties enable CuS to be used in light emitting devices and in biological labeling. It has now been recognized that coating the

nanocrystals of CuS by silica, not only makes them biocompatible but they also act as a biojunction. In core shell structure due to p-type semiconducting material it has been used as a core for aforementioned applications [9]. Moreover it has recently been reported that CuS (in nanorods morphology) shows 50% transmittance of visible light (300-650 nm). Transparency of these nanorods in the UV and near IR region indicates the potential future prospects of CuS in spectrally selective window coatings [10].

CuS has been fabricated over the years by a wide variety of synthetic protocols available in the material science and its applications (wherever possible) have also been discussed. Fabrication procedures of CuS under the headlines of solvothermal route, aerosol methods, solution methods and thermolysis with photocatalytic, photoharvesting [10], gas sensing [11], semiconducting and cancer therapeutic applications [12] are discussed.

1.1 Fabrication of CuS

1.1.1 Solvothermal Routes

Hydrothermal method produces binary inorganic materials in hot water under high pressure. The reaction is carried out inside an autoclave (steel vessel) which can bear the drastic conditions of temperature and pressure. The use of hydrothermal method in preparing metals or metal sulphides has become a recent trend due to the advantages associated with this method in terms of comparatively low temperature requirement, reproducibility, homogeneity and purity of the product.

Different research groups have reported the changes in morphologies and sizes by changing the precursors, concentration of the precursors, reaction conditions (temperature and pressure) and reaction times [13]. It has been reported that 3D flower like structures can be synthesized by a hydrothermal method using Cu_2O hollow

microspheres as template. Reaction of Cu_2O hollow spheres with thioacetamide at 40 ˚C for 2 h followed by hydrothermal treatment at 120 ˚C for 12 h results in high yield of 3D flowerlike structures with diameter ranging from 200 to 300 nm **(**Figure 1.2a&b). Cu_2O precursor was synthesized by the reaction of 25 ml of 0.05 M $CuSO_4$ solution and 1 g of PVP-K90 (Polyvinylpyrrolidone) in a conical flask under magnetic stirring at room temperature; pH was maintained at 10 with NaOH, under continuous drop wise addition of hydrated hydrazine as capping agent for 30 minutes on heating. Cu_2O and thioacetamide in stoichiometric amounts were then reacted inside the autoclave to produce the black precipitates of CuS which were separated from the reaction mixture after centrifugation (4000 rpm for 5 min) and purified by dispersing them in water [13].

Fabrication of CuS nanoparticles (NPs) (Figure 1.2c) without specification of morphology does not require any template, and in this regard, copper nitrate trihydrate, thiourea and water (as a solvent) have been used as a source of copper and sulphur respectively [3].

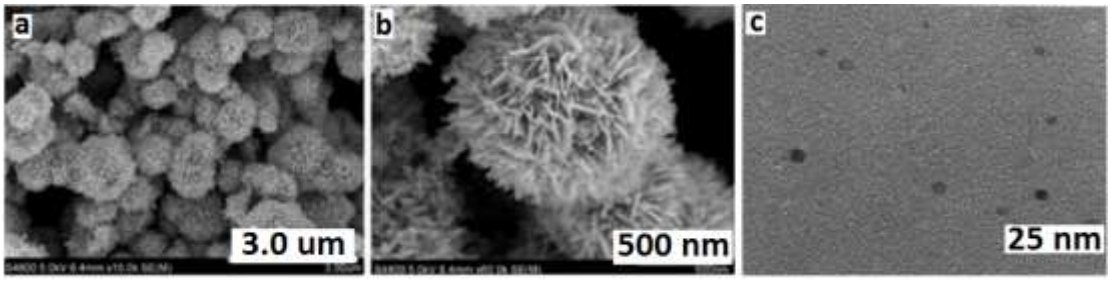

Figure 1.2a&b) SEM images of hierarchal CuS flower like submicrospheres. Modified with the permission of Lihua Wang et al. Bull. Mater. Sci. 2008,7,31. Copyright Indian Academy of Science **c)** TEM image of CuS nanoparticles. Modified with the permission of X Dong et al. Ind. Eng. Chem. 2002, 41, 4489-4493. Copyright American Chemical Society.

Another group has used copper salicylate as the source of Cu and thioglycolic acid as the source for sulphur for the fabrication of CuS with similar type of the experimental procedures reported in the previous two paragraphs [1].

Previously Roy and Srivastava have been succeeded to fabricate CuS nanowires (Figure 1.3a&b) from Cu-dithiooximide (DTO) (a novel single source precursor) by hydrothermal method at 120 ˚C for 24 h with a size range of 40-80 nm in diameter. The precursor was synthesized by reacting the separate solutions of 0.5 g of $CuCl_2.H_2O$ and DTO in 50 ml of ethanol under 2 h magnetic stirring with the addition of ammonium hydroxide to adjust the pH for precipitation. The stirring was carried out for 2 h which results in complete precipitation of the black colored Cu-DTO complex. The precipitates of Cu-DTO were filtered and washed with distill water/ethanol mixture and finally dried at 40 ˚C for 4 h. This process has an advantage in terms of air stability and in addition no capping agent has been used for the precipitation of CuS [4].

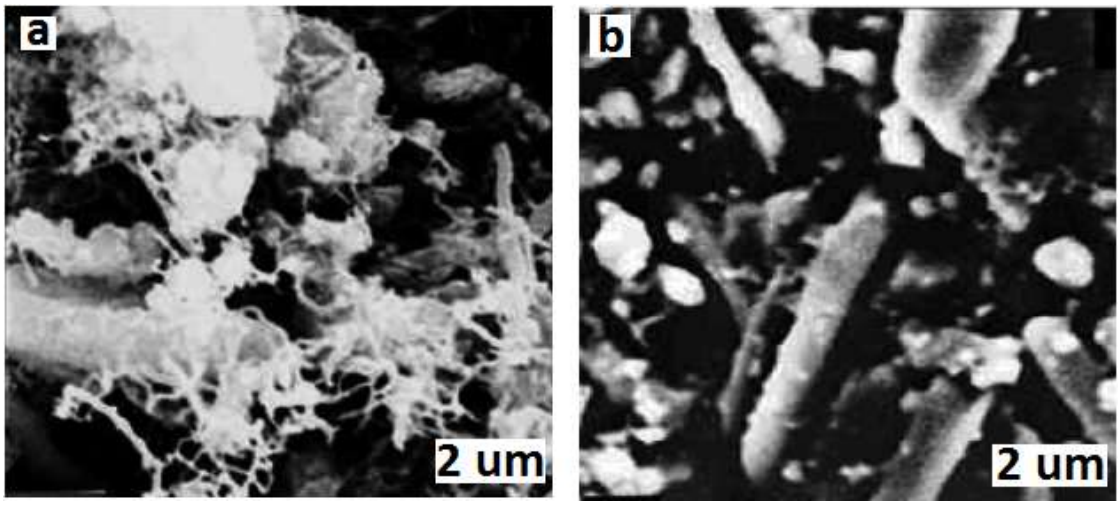

Figure 1.3a&b) SEM images of CuS nanowires. Modified with the permission of Poulomi Roy et al. Cryst. Growth & Des. 2006, 6, 8. Copyright American Chemical Society.

Microspheres (Figure 1.4a&b) of pineal CuS with thickness of 40 to 220 nm can be synthesized using pyridine as a solvent in a solvothermal process by the reaction of cupric chloride ($CuCl_2.2H_2O$) and thioacetamide (TAA, CH_3CSNH_2). In experimental 0.170 g (1 mmol) of cupric chloride ($CuCl_2.2H_2O$) was dissolved in 30 ml of pyridine under magnetic stirring at room temperature. As the solution became

transparent 0.150 g (2 mmol) of thioacetamide (TAA) were added. After ultrasonicating the reaction mixture at 60 ˚C for 15 min, it was transferred into a 50 ml teflon-lined autoclave and the apparatus was sealed carefully. Them the autoclave was heated in an electric desiccation at 180 ˚C for 15 h and the final product was collected as black precipitates which was washed with deionized water and ethanol and dried at 60 ˚C for 4 h under vacuum [14, 15].

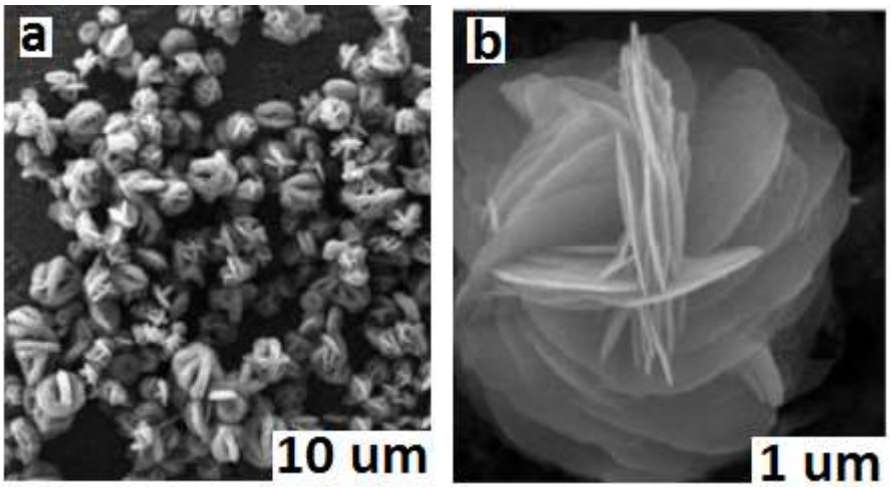

Figure 1.4a&b) SEM images of pineal microspheres. Modified with the Permission of K E Hanzhong et al. Mater. Sci. Ed. 2010, 25, 3.

It has been previously established that different ratios of capping agent can affect the shape and sizes of the materials fabricated. By using different ratios of L-cysteine to $CuCl_2.2H_2O$ different morphologies like dispersive flakes, flake built spherical aggregations, and solid microspheres can be synthesized. Under the hydrothermal conditions precursors decompose as self-sacrificial template to produce the interesting CuS nanostructures of high order and porous hollow microspheres. For the fabrication of these morphologies different amounts of L-cysteine (1 mmol, 2 mmol and 3 mmol) were dissolved separately in 10 ml of $CuCl_2.2H_2O$ aqueous solution (0.1 M) under constant magnetic stirring. 15 minutes stirring yielded deep blue, white and milky colored products depending upon the quantity of L-cysteine used. The products

were vacuum dried and autoclaved at 160-180 ˚C for 12 h. After this step the products were dispersed in water, filtered and then dried in vacuum after centrifugation [16].

CuS nanosphere (Figure 1.5a&b) with hollow interiors can be precisely synthesized by utilizing a novel two-dimensional coordination polymer which can be originally generated from a trinuclear building block $[Cu_3HSserine)_3(H_2O)_2].H_2O$. Three dimensional hierarchical flower-like CuS nanocrystals from the hydrogen-bonded metal complex $[Cu(H_2Sserine)_2].H_2O$ as a precursor may be understood from the spatial arrangement of the metal atom, and the organic ligand in the crystal lattice which plays a major role in determining the shape of nanomaterials. Ligand H_3Sserine was synthesized by reacting L-serine (1.0 mmol) in H_2O (10 ml) containing KOH (1 mmol) with the solution of salicyldehyde (1.0 mmol) in ethanol (10 ml). This results in a yellow solution which was stirred for 30 minutes at room temperature followed by cooling in ice bath. To this solution, addition of schiff base and $NaBH_4$ solution was carried out with gentle stirring until the yellow color disappeared, pH was adjusted using acetic acid and then the solid product was filtered and vacuum dried. Complex 1($[Cu_3HSserine)_3(H_2O)_2].H_2O$) was synthesized by reacting the ligand (1.0 mmol) with the solution of copper acetate (1.0 mmol) in 10 ml of water in the presence of Li(OH) (1.0 mmol). The resulting green colored solution contains the complex in the solution phase which may be rotary evaporated to have solid product. Complex 2 ($[Cu(H_2Sserine)_2].H_2O$) was also synthesized by following exactly the same procedure. The synthesized complexes were converted to CuS inside an autoclave which was supplemented by thiourea. The angular position of Cu (II) inside the complexes has been designated as a reason for difference in the morphologies [17].

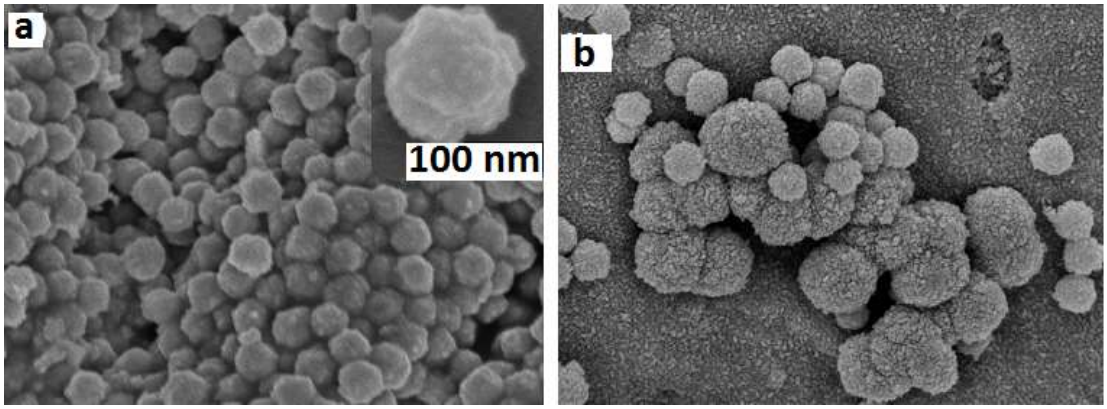

Figure 1.5a&b) FESEM images of CuS Nanospheres. Modified with the permission of Mangayarkarasi Nagarathinam et al. Cryst Growth & Des. 2009, 9, 10. Copyright American Chemical Society.

1.1.2 Aerosol Methods

Chemical vapor deposition method (CVD) is a chemical method which is used to produce high-purity and high-performance solid materials. Thin films in semiconductor industries are also made by this process. In (CVD) volatile precursors are frequently used which are reacted or decomposed on the substrate surface to deposit the desired product. The volatile products formed during the reaction are removed by gas flow through the chamber.

Thin films (Figure 1.6) of $Cu_\chi S$ have been reported by CVD using $Cu(thd)_2$ (thd = tetramethylheptanedionate), H_2S and H_2 as the precursors in a homemade low pressure CVD system. A deposition profile not caused by depletion of precursors is present in all films. Hydrogen is needed for growth to occur, in atomic layer deposition reaction between H_2S and $Cu(thd)_2$ [18].

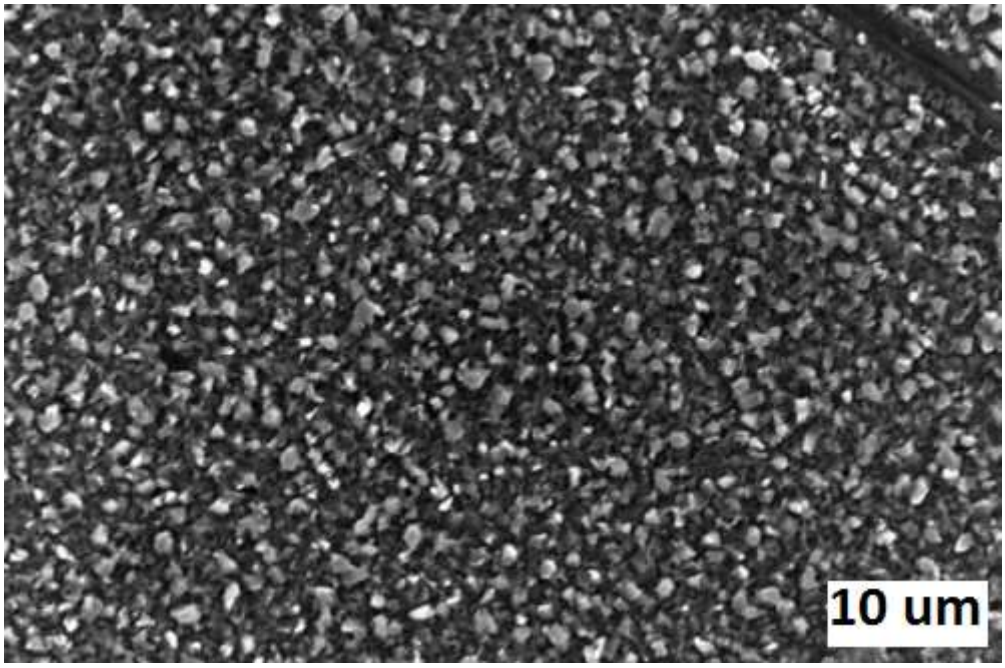

Figure 1.6) SEM image of CuS thin films. Modified with the permission of Reijnen et al. Chem. Mater. 2005, 17, 16. Copyright American Chemical Society.

Another modification of vapor based methods is the chemical vapor reactions with which single crystalline hexagonal CuS nano plates (Figure 1.7a&b) have been fabricated by reacting the sulfur vapor with copper films in a vacuum chamber at about 450 ˚C for about 7 h. Copper film with a thickness of 150 nm for nano-CuS deposition can be obtain by thermal evaporation of copper foil (99.999%) onto a silicon wafer in a vacuum (6.0×10^{-4} Pa) evaporation deposition apparatus. The vacuum CVR can be conducted in a homemade vacuum glass tube reactor. The copper film deposits on a Si substrate (about 0.5 × 0.5 cm) placed in the end-closed glass tube that should contain excess sulfur powder (about 100 mg, 99.999%) at the end of the tube. After evacuation seal the glass tube from the S powder end. Heat the seal glass tube to 450 ˚C in a tube furnace with a temperature increase rate of 5 ˚C min^{-1} and keep for about 7 h, cool the reaction system to room temperature [19].

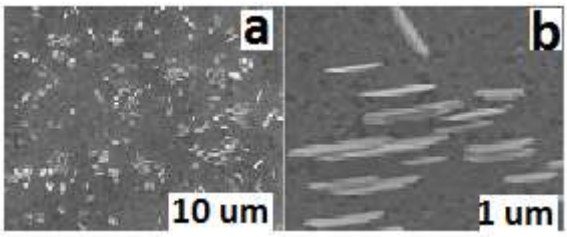

Figure 1.7a&b) SEM images of CuS Hexagonal Nanoplates. Modified with the permission of Ke-Ji Wang et al. Cryst. Growth & Des. 2007, 7, 11. Copyright American Chemical Society.

1.1.3. Solution Methods

Solution methods have their own importance for the synthesis of inorganic binary materials on the basis of homogeneous mixing of reactants, low temperature treatment, and easy processing. A facile, ionic liquid-assisted route has been developed to synthesize hierarchical CuS flower-like submicrospheres at 80 ˚C for 24 h. The method is based on the reaction of $CuCl_2$ and thioacetamide (TAA) in aqueous solution by using 1-n-butyl-3-methylimidazolium chloride ([BMIM]Cl) as a capping agent. CuS synthesis via an ionic route requires heating to 140 ˚C for about 10 minutes of 2 equivalents of 1-n-butyl-3-methylimidazolium chloride (4.8 mmol) with 1 equivalent of $CuCl_2.2H_2O$ (2.4 mmol). After cooling dark red, sticky liquid will be formed. To obtain homogeneous blue solution, dissolve sticky liquid in 4 ml of distilled water in a glass jar under constant stirring. Dissolve 0.18 g of TAA in 40 ml of distilled water and add in to the jar containing $CuCl_2$ solution gradually without stirring. Cover the jar and maintain at 80 ˚C for 24 h. This will result in a black solid product, filter and wash with distilled water/absolute ethanol in sequence, and then dry in a vacuum at 60 ˚C for 6 h [20-22]. Almost similar type of results has been achieved by using hexamethylinetetramine (HMA) and acetic acid as capping agent [23, 24].

In solution chemistry methods, a novel approach for the fabrication of CuS is the pressure leaching in which major copper sulphides such as chalcopyrite, bornite and

chalcocite undergo phase conversion to covellite (CuS) which is the most stable sulphide form of copper. Copper present in flotation concentrate has been observed to solubalize in the leaching solution only after the conversion of all copper sulphide minerals into covellite phase. During copper sulphide conversion permeable, openwork texture of covellite are formed which not only facilitates easy leaching but also favor the transport of the leaching medium to the leaching surface and help in leaching of the remaining minerals in the solid feed. For pressure leaching experiment, copper sulphide concentrate is fed in a Lubin concentrator which acts as a feed for further process. Leaching is conducted at temperatures of 100 ˚C, 120 ˚C, 140 ˚C, 160 ˚C and 180 ˚C. In each experiment 135 g of dry concentrate is introduced to the reactor in the form of water slurry and 0.8 L of solution acidified by means of sulphuric acid with an initial concentration of 120 gL^{-1}. After preliminary decomposition of carbonate matter (calcium and magnesium carbonates) with H_2SO_4 autoclave is sealed and purged three times with nitrogen. As temperature reaches up to 100 ˚C, nitrogen is removed from the reactor and remaining slurry is heated up again. When the required temperature is achieved then oxygen is introduced to the reactor by keeping the partial pressure of oxygen to a level of 5.0 atm and stirring rate to 400-450 rpm. Between temperatures of 100 ˚C to 160 ˚C there will be complications with the reactions inside the reactor and also difficulties in the determination of the balance of copper mineral content, so it is not useful for explanation of phase conversions. Although an increasing content of covellite in comparison to other minerals is observed but it is impossible to find out quantitative relationship between them. At 180 ˚C it is possible to perform qualitative and quantitative characteristics of the phase conversions taking place in the reactor and for that, first sample of slurry is taken (at time zero) when the temperature reaches up to just 180 ˚C (just before the introduction of oxygen to the reactor). For identification

of main mineral phases in the feed and in samples taken during leaching at 180 ˚C, they are prepared and polished for microscopic examinations in the reflected light [25].

CuS NPs have also been prepared by mixing the microemulsions (water/carbondioxide (W/C)) of $Cu(N0_3)_2$ and Na_2S using the sodium salt of bis(2,2,3,3,4,4,5,5-octafluoro-1-pentyl)-2-sulfosuccinate (di-HCF_4) surfactant as capping agent. CuS NPs ranging from 4 to 6 nm size can be produced by using water to surfactant ratio of 10 and a copper concentration of 7.8 mM in the aqueous phase. The electrolytes have no effect on the cloud-point pressures significantly, even at higher concentrations. A micro emulsion is a thermodynamically stable system in which two immiscible components generally water and oil (W/O) are dispersed as nanosize droplets (typically 5-25 nm in diameter) surrounded by a nano layer of surfactant molecules in the continuous hydrocarbon phase. Micelles droplets exhibit a dynamic exchange of their contents that facilitates the reactions of the reactants dissolved in different droplets [26].

CuS nanotubes (Figure 1.8a &b) with good morphological and high chemical purity can be prepared using [Cu(thiourea)]Cl.1/2H_2O nanowire precursors as self-sacrificial templates at room temperature. Well-organized [Cu(TU)]Cl.1/2H_2O with good morphology and high purity can be prepared directly by mixing an aqueous solution of $CuCl_2$ with thiourea at room temperature. Depending on the initial concentration of thiourea and $CuCl_2$ well-aligned [Cu(TU)]Cl.1/2H_2O nanowires dandelion or thorn like architecture are in hand [27].

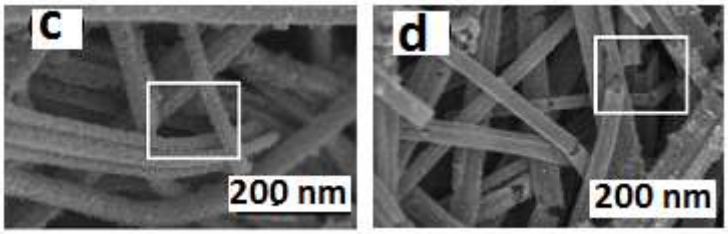

Figure. 1.8a &b) SEM images of CuS Nanotubes. Modified with the permission of Jianfei Mao et.al. Cryst. Growth & Des. 2009, 9, 6. Copyright American Chemical Society.

A new route to synthesize nanocrystals of covellite, is to use a hydrogen-bonded 1D coordination polymer, $[[Cu(HSglu)(H_2O)].H_2O]_n$ (glutamic acid = glu) as a precursor which will itself act as a sacrificial template. There is a remarkable correlation between the repeating patterns of the metal in the coordination polymer with the preliminary shape of the obtained CuS. For the fabrication of CuS, solid precursor (50.0 mg) was mixed with thiourea (54.3 mg) inside an autoclave using 25 ml of water as the reaction medium. This reaction mixture was placed at the desired temperature for a specific time to have information about the morphologies and shapes of the CuS formed. Different morphologies of CuS have been attributed to the noncovalent interactions of reduced schiff base in the form of hydrogen bonding [28].

Another very simplified solution chemistry approach is the soft template method which involves the use of CS_2, Na_2S and $CuSO_4$ as the source for sulphur and copper respectively. Experimental procedure involves the reaction of 15 ml Triton X-100, 25 ml cyclohexane and $CuSO_4$ aqueous solution (0.5 M) in a flask to form the micro emulsion solution. 15 minutes stirring by the addition of CS_2 (0.5 M) under reflux for 4 h gives brown color appearance which is an indication for the formation of CuS. Reaction flask was cooled to room temperature and precipitated product was filtered and vacuum dried [29].

CuS twinned nanorods (Figure 1.9a&b) can be synthesized by wet chemical in situ source-template-interface reaction (ISTIR) method, at low temperature (105 ˚C). The reaction is carried out by mixing CS_2 with $CuCl_2.2H_2O$ (0.253 g) in the presence of 2 ml of ethylene diamine (en) in a flask under constant magnetic stirring for 15 minutes. Change in color from colorless to green confirmed the formation of $[Cu(en)_2]^{2+}$ complex. Refluxing the whole solution at 105, 120, and 140 ˚C for 12 h, provided black color product which was washed with distil water and ethanol and then dried in a vacuum at 60 ˚C for 4 h [30].

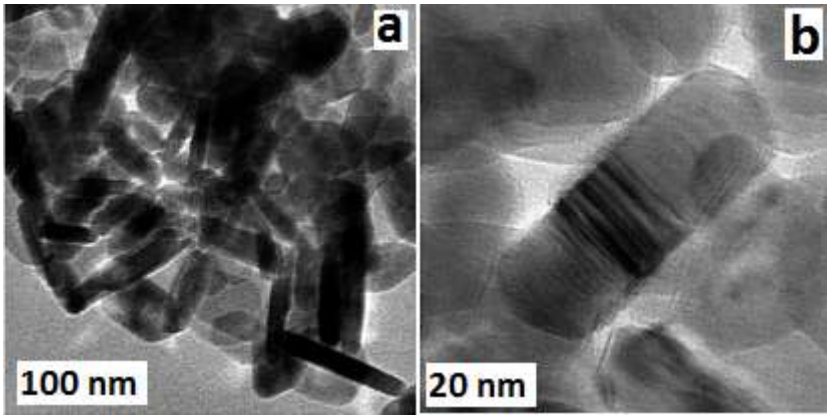

Figure 1.9a&b) TEM images of Cus Twinned Nanorods. Modified with permission from Poulomi Roy et al. Cryst. Growth & Des. 2008, 5, 8. Copyright American Chemical Society.

Another important, old but simple technique for the fabrication of binary inorganic materials, is the chemical bath deposition. This technique is generally adopted for the formation of thin films of inorganic materials. Nillohit et al. [31] have reported the fabrication of CuS by this method using copper acetate and thiourea as a source for copper and sulphur respectively in the presence of triethanolamine (TEA) as a surface active agent. TEA also functions as a complexing agent and pH modulator inside aqueous medium. Experimental of this technique is very much simple which involves the simple mixing of the precursor and only one minute stirring for

homogeneity. Placement of clinical glass slide in this reaction mixture for 18-20 h, coats very uniform CuS on them [31].

Another important morphology of CuS is the CuS cages fully exposed with nanotwinned building blocks (Figure 1.10) which was fabricated in a successful attempt using cubic Cu_2O as a template to produce Cu_2O/CuS core/shell architectures by reacting (0.6 g) of Cu_2O template to a mixed anhydrous ethanol solution (150 ml) consisting of Na_2S (0.36) and NaOH (0.006 g), at room temperature for almost 10 minutes under constant magnetic stirring. The resulting precipitates were separated by centrifugation and then washed with distill water and absolute ethanol. In the next step CuS hollow cages with nanotwinned building blocks were in hand by the introduction of core/shell particles (made in the 1st step) to the ammonia solution (25%) for 120 h which resulted in the removal of inner Cu_2O cores. The particles were centrifuged twice and then washed with distilled water and absolute ethanol respectively and dried in a vacuum at 60 ˚C for at least 12 h. Finally the hollow cages of CuS were synthesized without nanotwinned building blocks by dissolving the template Cu_2O to a solution of Na_2S (0.36 g) and NaOH (0.006 g) at room temperature under constant stirring for 10 minutes. The resulting precipitates were separated by centrifugation and then washed with distilled water and absolute ethanol. The Cu_2O/CuS core/shell particles were placed in 25% ammonia solution for 120 h which removed the Cu_2O cores. The obtained particles were centrifuged and then washed with distill water and absolute ethanol, and finally dried in vacuum at 60 ˚C for 12 s [32].

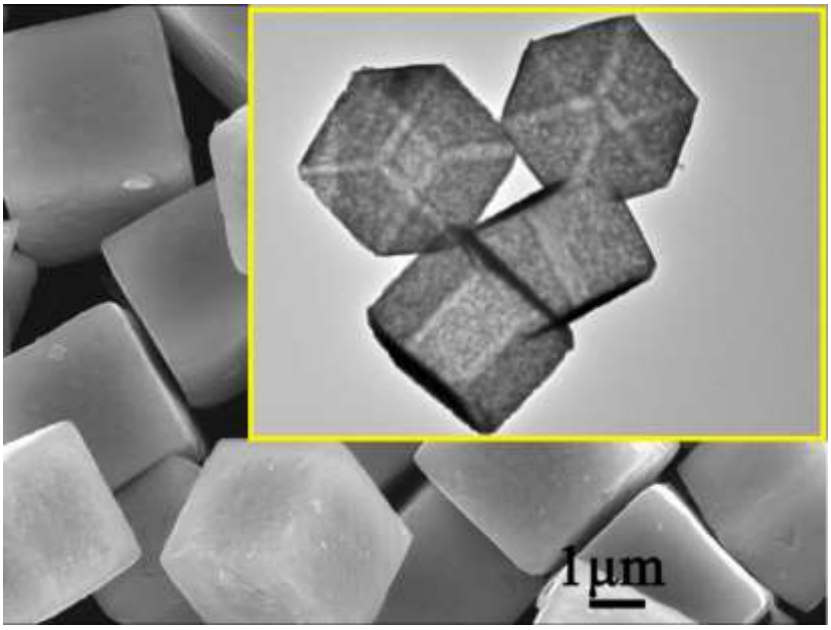

Figure 1.10. FESEM image of the cubic Cu_2O templates. Yellow inset represents TEM image of the cubic CuS cages without nanotwinned building blocks. Modified with permission of Shaodong Sun et al. Cryst. Eng. Commun. 2012, 14, 67. Copyright Royal Society of Chemistry.

1.1.4 Thermolysis

Thermolysis is one of the simplest methods for inorganic synthesis and only involves the placement of materials inside the furnace at desired temperature in an environment (gas/vacuum) required. Core-shell microspheres (Figure 1.11) can be made from hexagonal CuS by thermolysis of $Cu(R_2dtc)_2$ (where R=octyl and dtc=dithiocarbamate) precursor at 130-180 ˚C under N_2 flow for 0.5 h. Copper complex was synthesized by the reaction of di-n-octylamine (20 mmol) with NaOH (20 mmol) in methanol under constant magnetic stirring until clear solution. Then the addition of CS_2 (40 mmol) was carried out in a drop wise manner below 4 ˚C for 4 h. In another beaker copper nitrate (9.8 mmol) was dissolved in 20 ml of distilled water and 20 ml of dichloromethane and then this solution was stirred with the above solution for 0.5 h. Black colored solid precipitates were filtered and vacuum dried. For the production of CuS the synthesized complex was thermolysed in a pyrex boat capped from both ends

inside a tube furnace. The tube was purged with N_2 for 5 minutes and after that the complex was heated at 180 ˚C for 30 minutes. The solid residue obtained was dispersed in dichloromethane to remove the impurities and after wards dried in vacuum after centrifugation for 5 minutes [33].

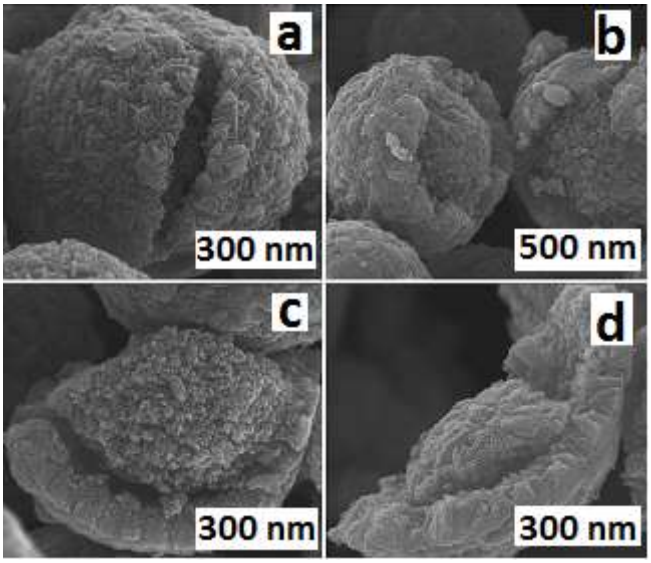

Figure 1.11a, b, c &d) SEM images of core shell CuS microspheres. Modified with the permission of Yu-Bhio Chen et al. Cryst. Growth & Des. 2008, 8, 8. Copyright American Chemical Society.

Chemical deposition (CD) is another method which is being used for the formation of inorganic materials. And if single source precursor is used during CD it has its own importance in terms of better stoichiometry control and good safety arrangements. Maji et al. have used CD with a single source precursor $[Cu(SOCCH_3)_2Lut_2]$ for the fabrication of CuS thin films successfully [34]. Experimental was performed by spreading the drops of the complex solution on glass slides and then pyrolyzing the solution at 350 ˚C.

1.2 Applications of Copper Sulphide

1.2.1 CuS for Ablation of Cancer Cells

Photothermal ablation (PTA) therapy has attracted much interest in the recent years as an alternative to surgery and chemotherapy for therapeutic intervention of specific biological targets. Laser-induced PTA in near-infrared (NIR, λ = 700-1100 nm) effectively converts NIR optical energy into thermal energy and has attracted increasing attention, because the NIR laser is absorbed less by biological tissues and a typical penetration depth of the NIR (such as 980 nm) light can be several centimeters in biological tissues. A prerequisite for the development of NIR laser-induced PTA is to gain access to biocompatible and efficient photothermal agents. Semiconductor CuS is one of the latest developing and promising photothermal coupling agent along with Au CNTs (carbon nanotubes). CuS having an advantage of low cast, low toxicity and intrinsic NIR region absorption derived from energy band transitions instead of surface plasmon resonance. The use of metal chalcogenides as plasmonic-active semiconducting material illustrates that it is not a stringent condition for material to contain a metal deficient lattice. The hexagonal covillite CuS that is a stoichiometric member of broad family of copper sulphides exhibit a particular crystal habit and unique metal like properties that accounts for its P-type anisotropic conductivity. The proposed models of CuS electronic band structures suggest that CuS has the ability to allow intrinsically a significant density of valence band delocalized holes without further need of significant metal vacancies in the crystal lattice. It is intrinsic property of CuS to incorporate sufficient cation vacancies due to high activation energy for their formation and slow diffusion of cations within the lattice. It is now believed that in nanostructural form of CuS acts as an unconventional material which has vacancies without doping and can support composition independent localized surface plasmon resonance. It is exclusively correlated with its geometry and metallic like nature [35]. Recently Tian and Tang [12] have developed CuS nanoparticles as a new photothermal

coupling agent for PTA of cancer cells in vitro and in vivo, under an irradiation of 808 nm laser with a power of 16 and 24 Wcm^{-2}, which suggests that CuS nanomaterials have a great potential to revolutionalize photothermal agents. But one of the limitation of CuS nanoparticles as a photothermal agent is their low photothermal conversion efficiency, and the 808 nm laser power intensity (16 and 24 W cm^{-2}) require to cause sufficient cell death of in vitro nanolayer setting which is approximately 48 and 72 times higher than the conservative limit of 808 nm laser intensity setting for human skin exposure.

1.2.2 CuS in Lithium Ion Batteries

CuS is widely used as high capacity cathode material in lithium secondary batteries. In these batteries the capacity of cathode material is much lower as compared to anode material [7]. CuS has good electronic conductivity (10^3 $S^{-1}cm$) and high energy capacity (560 $mAh^{-1}g$). These properties enable CuS to be used as a cathode material in lithium batteries. Several attempts have been made to use CuS as a cathode in lithium rechargeable batteries. Hughes et al. has discussed that main problem with this cathode material (Li/CuS) is, the rapid decrease in the capacity. Exner and Hep have used 1 M $LiCF_3SO_3$/1,3-dioxolane electrolyte in Li/CuS coin cell which results in only 50% charge capacity. The EVS diagram indicates that discharging reactions take place at 2.05 and 1.68 V, and for the charging reaction the corresponding peaks appear at 1.85 and 2.25-2.41 V (Figure 1.12a). These peaks indicate that the capacity of each peak (257 and 264 $mAh^{-1}g$) during the discharge reaction is almost same in the 1st cycle whereas during charging, capacity of higher voltage peak (350 mAh^{-1} g) is much larger than the peaks at lower voltage (21$mAh^{-1}g$) (Figure 1.12b). The voltage profile for peak 2 (Figure 1.12b) plateau shows that the discharging reaction consists of 2 steps whereas the charging reactions are complicated. There is a difference of 40 $mAh^{-1}g$ in the

theoretical (560 $mAh^{-1}g$) and experimental (520 $mAh^{-1}g$) discharge capacities however charging capacities are 66% and 71% of the theoretical values [7].

The XRD pattern for discharge reaction (Figure 1.12c) does not change from the open circuit voltage (OCV) at 1.8 V, which indicates the insertion of lithium ions to CuS lattice during the 1st voltage plateau and it indicates the formation of homogeneous Li_xCuS phase, and change in XRD pattern starts from 1.68 V which is the exact position of 2nd voltage plateau. The diagram also represents the Bragg peaks for djurleite ($Cu_{1.96}$ S), Li_2S and metallic copper. By decreasing the voltage further to 1.5 V, which is below the second voltage plateau only Li_2S and Cu peaks are present which indicates that most of the $Cu_{1.96}S$ has been changed to Li_2S and Cu. Again charging from 1.5 to 2.0 V djurleite appears but Li_2S and Cu remain and don't disappear at this potential. The chalcocite or djurleite transforms in to a series of copper sulphides during oxidation which corresponds to voltage of 2.3 to 2.4 V, and all the peaks disappear at 2.45 and 2.46 V but a broad peak for CuS emerges with a low intensity which clearly indicates the transformation of Cu an Li_2S in to CuS [7].

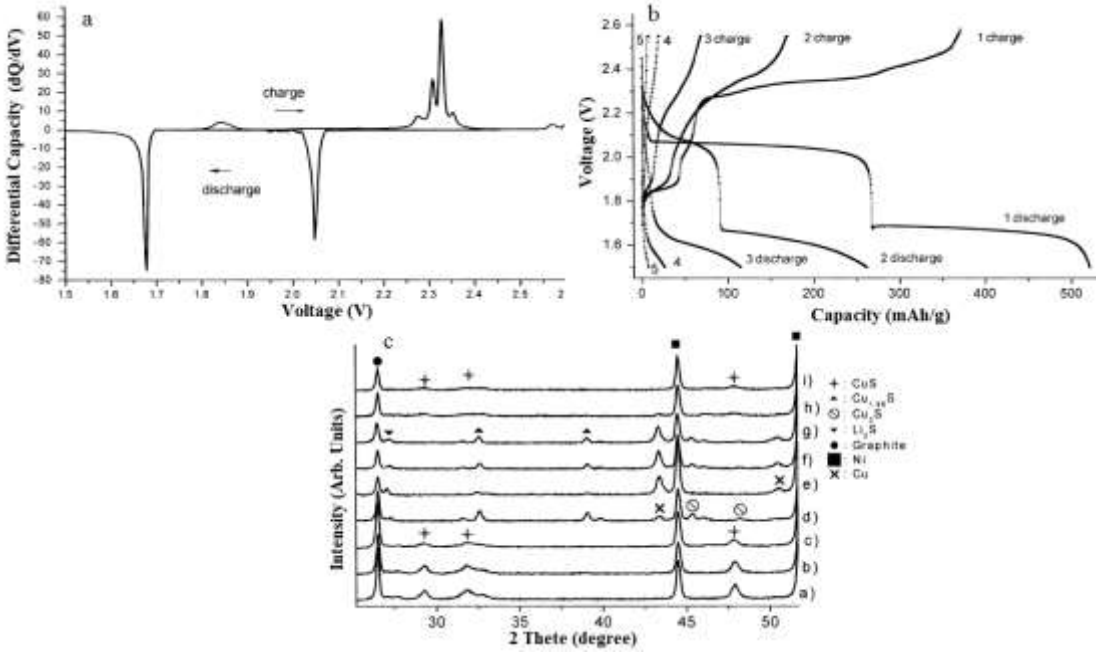

Figure 1.12. a) EVS diagram of CuS electrode. **b)** Behavior of high purity CuS electrode during 5 cycles between 1.5-2.6 V ranges at room temperature. **c)** XRD patterns of CuS electrode during the 1st cycle a) OCV, b) discharge to 1.95 V, c) discharge to 1.8 V, d) discharge to 1.68 V, e) discharge to 1.5 V, f) charge to 2 V, g) charge to 2.27 V, h) charge to 2.45 V, i) charge to 2.60 V. Modified with permission of Chung, J. S. et al. J. Power Sources 2002, 108, 226 Copyright Elsevier.

1.2.3 Cus in Gas Sensing

CuS is generally not known for gas sensing but its golf balls like morphology (Figure 1.13 a&b) has shown gas sensing properties mainly because of its high surface area, more active sites and hollow structure in three dimensions. These golf balls have an emission band at 460 nm (Figure 1.13c) and have the ability to sense the ammonia gas at a concentration level of 480 ppm, which is far less than its fetal dose (3500-7000 mgm^{-3}). Figure 13d shows that the PL intensity is fully reversible within a short time after the removal of the gas from the detector. The response amplitude of CuS golf balls (0.12) was found larger than that of single-walled Cu_7S_4, but smaller than that of double-walled Cu_7S_4 nanobox. Also the response time of the golf balls is 33 s which is less than the recovery time i.e. 44 s and interestingly both the response time and the recovery time of the CuS golf balls are smaller than that of the single-walled as well as double walled Cu_7S_4 which is due to the special microstructure and highly porous nature of the golf balls [11].

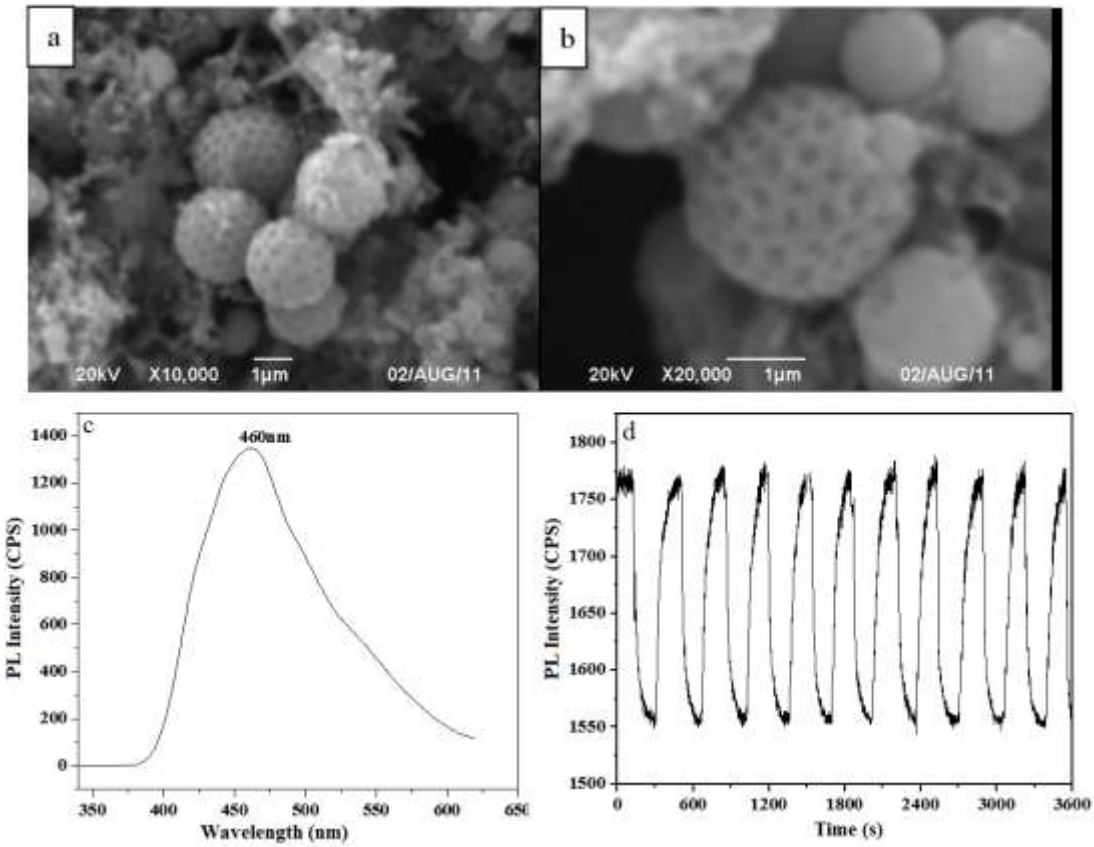

Figure 1.13. SEM images of as-prepared CuS golf balls. **a)** Low magnification, **b)** High magnification, **c)** PL emission spectra of CuS, **d)** Room temperature time profilesof PL intensity of sensors based on CuS golf balls to NH_3.

1.3 Photocatalytic Degradation of Organic Dyes

Today the most serious threat to humanity is the global warming. Our world is facing uneven climatic changes which results in disasters around the world such as droughts, heat waves, severe storms and rising seas and floods all over the world [36-39]. The major threat to environment is the discharge of different dyes from different sources (e.g., paper and pulp industries, textile industries, dye and dye intermediates industries, tanner, pharmaceutical industries and craft and bleaching industries) which are introducing huge amount of dyes in natural water as well as waste water treatment systems [40]. 50-100 L wastewater/kg is produced by dyeing and finishing industry [41], Vinu et al says that without any proper physiochemical treatment about 10-15%

of 700 thousand tons of 10 thousand different types of dyes are discharged into different water systems and are increasing day by day [42]. About one million tons of dyes are produced worldwide annually and there are more than 100,000 commercially available dyes [43-45]. The reactive dyes have very low fixation rate and these dyes are estimated to contribute the major part in the waste water which reach to almost 57 thousand tons. Fixation rate of dye is influenced by the extent of hydrolysis [46] and toxicity of these dyes cause negative effects on the environment which in turn effect human health. The negative impact include both non biodegradability of dyes as well as their high color intensity which results in large decrease in aquatic life by blocking sunlight [47]. Their removal is necessary because most dyes and their breakdown products are toxic, carcinogenic or mutagenic thus affects life directly. These dyes cause irritation of the respiratory tract, eyes, skin, asthma, sore throat and allergic contact dermatitis [48]. The persistent dyes will remain in the water for long time because they are non-biodegradable and also resistant to light [49]. In paper and textile industries several methods were studied to remove these dyes but traditional methods are not efficient to decolorize these dyes [50]. Wastewater treatments for color removal can be divided in to 3 major categories including chemical, physical and biological treatments [51, 52]. All the above mentioned techniques have their limitations in industries.

1.3.1. Dye removal techniques

Liquid phase adsorption is the most well-known process for dye removal from waste water. The adsorption is an equilibrium separation process which is very efficient if the sorbent is cheap in terms of cost, simplicity to design, flexibility and insensitivity to toxic pollutants. The decolorization process depends on physiochemical factors (e.g. interaction between sorbent and dye, reaction time, particle size, surface area of sorbent, temperature and pH) [53]. Another widely used process to remove dyes is the use of

activated carbon [54, 55]. But use of activated carbon is somewhat critical because of high cost and regeneration problems of carbon [37]. The main difficulty in regeneration is desorption of the adsorbed dye from the surface of activated carbon. In addition to these techniques several filtration techniques are widely used for dye removal these include microfiltration, ultrafiltration, and some time reverse osmosis [56, 57]. However membrane filtration processes are associated with some disadvantages among these they can be only applied in small flow rate, high cost and require membrane to push the waste water flow through membrane filtration. Biodegradation of dyes is also used as an efficient method and is an alternative to both physical and chemical processes. Viruses, bacteria and algae are used as microorganism for this purpose. They are involved in microbial degradation, fungal decolorization, bioremediation systems and adsorption by microbial biomass [44, 58]. However this technique is limited by the fact that some chemicals are too toxic that results in decrease in number of active microorganisms and long hydraulic retention time [58].

In chemical treatment coagulation and flocculation are normally used for separation of dyes. These techniques are associated with some disadvantages which include high cost of the coagulating and flocculating agents, pH dependence of some dyes for their removal and waste disposal after accumulation of concentrated sludge. Secondary pollutants may arise due to excessive use of some chemicals. Chemical treatment involves ion exchange process which is not efficient in removing several types of dyes. Rate of reaction is limited by diffusion rate and solvents use for regeneration are very expensive [51].

1.3.2 Photo catalytic degradation of dyes

In the 20^{th} century photocatalytic systems gain much interest in solving environmental problems especially in getting rid of residual dyes from wastewater and

other polluted systems [37, 59, 60]. Photocatalytic systems are considered to be green environmental solution for better future environment. For this purpose several photocatalytic systems have been introduced which include metal oxides, metal sulfides and metal selenides. All these systems are effective for photochemical degradation of different dyes.

1.3.3 Metal sulfides for dye degradation

1.3.3.1 CuS Nanoparticles

Copper sulfide exist in different morphologies which have different band gaps e.g. CuS microspheres, nanotubes, nanoflakes and nanoparticles have band gap of 2.08 eV, 2.06 eV, 2.16 eV and 1.88 eV respectively. In the presence of H_2O_2 all morphologies of CuS acts as a catalyst and not a Photocatalyst it is well explained by the fact that during dark there is only 2-3% decrease in the degradation of dye initially but as the reaction proceeds there will be no difference in the activity as shown in the table 1.1.

Table 1.1: Comparison of MB degradation (%) in the dark and in the presence of light using CuS Nanotubes and Microspheres with H_2O_2 [61]

Duration (min)	**CuS nanotubes (dark) (%)**	**CuS nanotubes (light) (%)**	**CuS microspheres (dark) (%)**	**CuS microspheres (light) (%)**
5	52.4	54.9	79.0	82.2
10	77.0	82.9	96.1	97.3
15	94.4	92.8	97.1	98.0
20	97.6	97.4	97.2	98.4

Another group reported the dye degradation activity of CuS stacked plates towards different dyes. CuS has strong absorption bands in the visible region considering this under various pH conditions cationic dyes like methylene blue MB, malachite green MG, rhodamine B RhB , anionic dye like methyl orange MO, eosin E and neutral dye methyl red MR were chosen to examine their photodegradation. In case of MB successive decrease in the absorption peak at 663 nm was observed. From kinetics of reaction it is observed that degradation activity is quite faster for cationic dyes like MB, MG and RhB and minimum for anionic or neutral dye [62,63].

The list of Metal sulfides and their hybrids for dye degradation is listed in Table 1.2.

Table 1.2.Room temperature catalytic studies on the degradation of dyes with Metal sulfides and their Hybrids under UV/visible light

Catalyst	**Band gap (eV)**	**Dyes**	**Working volume/conc.**	**Amount conditions**	**EMR range nm**	**Efficiency %**	**Reference**
FeS_2 films	2.7	RB	6.6×10^{-6} M	20 mg 100 W tungsten lamp	546 nm	84 (300 min)	[64]
FeS_2 nanoparticles		MB	6×10^{-6} M	20 mg Tungsten halogen lamp 200 W	664 nm	86	[65]
CoS nanoparticles	1.10	MB	25 ml of 0.25 ppm	125 W mercury lamp	664 nm	34 (70 min)	[66]
CoS/AIMCS-41				100 mg		90 (20 min)	
CoS/PAN		MB			664 nm	90 (80 min)	[67]
		MR			430 nm		

CuS nanotubes CuS nanospheres CuS stacked plates	2.06 2.08 2.2	MB MB	40 ml 2×10^{-5} M 30 ml 10^{-5}	10 mg 0.01 g	663 nm 663 nm	97.4 (20 min 98.4 (20 min) 98 (30 min)	[61] [62, 63]
Ag2S nanoparticles Ag2S/MCM-41	1.08	MB	25 ml 0.16-0.32 ppm	0.02-5g/L UV lamp	664 nm	41(60 min) 94 (60 min)	[68]
ZnS cubic nanoparticles ZnS nanoribbons ZnS nanoparticles Rod shape ZnS/thioglycolic acid ZnS naoparticles/(2-10 %Ni,Mn,Cu)	3.66	Safranine T XB-3B Safranin O MO 2,4-NP MO Safranine	10 mg/L 15 ml of 25mg/L 50 % 100 ml of 10mg/L 5mg/L	20 mg UV lamp 1 piece UV lamp 50 % Xe lamp 20 mg 300 W mercury lamp 150mg/L 100 W mercury lamp 0.25 g 450 W Xe arc lamp	254 nm 588 nm 520 nm 661 nm 661 nm 519 nm	More than 80(30 min) 88.4 (100 min) 51 (40 min) 94(60 min) 54(60 min) 95.2(30 min) 93.4(30 Min) 84 (3 h) 65 (3 h) 87 (3 h)	[69] [70] [71] [72] [73] [74]

ZnS nanparticles/Thioglycerol		Reactive red Bromo phenol blue Crystal violet	100 ml of 10 mg/L		324-600 nm		
CdS hollow spheres	2.4	MB	50 ml of 44 ppm	50 mg 300 W Xe lamp	660 nm	87 (60 min) 100(480 min)	[75]
		RhB	50 ml 1×10^{-5} M	50 mg 350 W Xe lamp	553 nm	100 (45 min)	[76]
CdS/1.2 % Ni		RhB	50 ml 1×10^{-5} M	50 mg 350 W Xe lamp	553 nm	100 (35 min)	[77]
thioglycolic acid (CdS-T), potassium pyrosulfate (CdS-K), disodium salt of EDTA (CdS-E)	2.96 2.66	MB	200 ml	0.1 g 160 W mercury vapour lamp 25 mg Sun Light	663 nm	87 (105 min) 88(105 min) 32 (105 min) 100 (150 min)	[78] [79]
$CdS/CdTiO_3$	2.63	MB	50 ml of 10 ppm		664 nm		

Bi_2S_3/BiOCl Bi2S3/thiogly colic acid	1.3	RhB MR	50 ml 20 ml of 10 mg/L	0.03 g 500 W Xe lamp 10 mg 300 W mercury lamp	553 nm 661 nm	98 (120 min) 96 (4 h)	[80] [81]
SnS2 nanosheets	2.2	RhB	5 ml of 0.01 mM	2mg Sun Light	553 nm	93 (40 min)	[82]
NiS-Clinptilolite	0.5	Furfural EBT	330 mg/L	330 mg/L 75 W Hg lamp		60(240 min)	[83, 84]

1.4 Objectives

Copper sulphide is a binary inorganic material and acts as a catalyst for dye degradations and have potential applications in lithium ion secondary batteries. Keeping these facts under consideration it was estimated that copper sulphide can act as a photocatalyst under direct sunlight (outdoor lightening) because it has the ability to absorb solar light of 400-600 nm. The solar light bears sufficient energy to eject electron from valence band of copper sulphide and photocatalytic process will be economical because no efforts are required to produce energy.

Keeping these significance in view, research plan was

- To synthesize copper sulphide through single source precursor.
- To synthesize copper sulphide under moderate conditions in which no capping agent was involved.
- To carryout photodegradation of organic dyes.

- To carryout battery applications against li as a counter electrode.

References

[1] M. Salavati-Niasari, S. Alizadeh, M. Mousavi-Kamazani, N. Mir, O. Rezaei, E. Ahmadi, J. Clust. Sci., 24 (2013) 1181-1191.

[2] M. Saranya, C. Santhosh, S.P. Augustine, A.N. Grace, J. Exp. Nanosci., 9 (2014) 329-336.

[3] M. Saranya, C. Santhosh, S.P. Augustine, A.N. Grace, J. Exp. Nanosci., (2012) 1-8.

[4] P. Roy, S.K. Srivastava, Cryst. Growth. Des., 6 (2006) 1921-1926.

[5] J. Folmer, F. Jellinek, J. Less. Common. Metal., 76 (1980) 153-162.

[6] R.S. Mane, C.D. Lokhande, Mater. Chem. Phys., 65 (2000) 1-31.

[7] J.-S. Chung, H.-J. Sohn, J. Power. Source., 108 (2002) 226-231.

[8] W. Liang, M.-H. Whangbo, Solid. State. Commun., 85 (1993) 405-408.

[9] M. Darouie, S. Afshar, K. Zare, M. Monajjemi, J. Exp. Nanosci., 8 (2013) 451-461.

[10] M. Basu, A.K. Sinha, M. Pradhan, S. Sarkar, Y. Negishi, T. Pal, Environ. Sci. Technol., 44 (2010) 6313-6318.

[11] J. Xu, J. Zhang, C. Yao, H. Dong, J. Chil. Chem. Soc., 58 (2013) 1722-1724.

[12] Q. Tian, M. Tang, Y. Sun, R. Zou, Z. Chen, M. Zhu, S. Yang, J. Wang, J. Wang, J. Hu, Adv. Mater., 23 (2011) 3542-3547.

[13] D. Wu, Y. Wang, C. Zhang, H. Zhu, Procedia. Eng., 36 (2012) 25-33.

[14] W. Luo, X. Tian, Z. Pi, J. Wuhan. Uni. Technol-Mater. Sci. Ed., 25 (2010) 459-463.

[15] J. Liu, D. Xue, J. Cryst. Growth, 311 (2009) 500-503.

[16] B. Li, Y. Xie, Y. Xue, J. Phys. Chem. C, 111 (2007) 12181-12187.

[17] M. Nagarathinam, K. Saravanan, W.L. Leong, P. Balaya, J.J. Vittal, Cryst. Growth Des, 9 (2009) 4461-4470.

[18] L. Reijnen, B. Meester, F. de Lange, J. Schoonman, A. Goossens, Chem. Mater., 17 (2005) 2724-2728.

[19] K.-J. Wang, G.-D. Li, J.-X. Li, Q. Wang, J.-S. Chen, Cryst. Growth. Des., 7 (2007) 2265-2267.

[20] J. Xu, X. Cui, J. Zhang, H. Liang, H. Wang, J. Li, Bull. Mater. Sci., 31 (2008) 189-192.

[21] C. Chen, Q. Li, Y. Wang, Y. Li, X. Zhong, Front. Optoelect. China, 4 (2011) 150-155.

[22] L. Ge, X.-y. Jing, J. Wang, S. Jamil, Q. Liu, D.-l. Song, J. Wang, Y. Xie, P.-p. Yang, M.-l. Zhang, Cryst. Growth. Des., 10 (2010) 1688-1692.

[23] S. Wang, J. Ning, L. Zhao, B. Liu, B. Zou, J. Cryst. Growth., 312 (2010) 2060-2064.

[24] I. Puspitasari, T. Gujar, K.-D. Jung, O.-S. Joo, Mater. Sci. Eng. B, 140 (2007) 199-202.

[25] A. Muszer, J. Wódka, T. Chmielewski, S. Matuska, Hydrometallurgy, 137 (2013) 1-7.

[26] X. Dong, D. Potter, C. Erkey, Indian. Eng. Chem. Res., 41 (2002) 4489-4493.

[27] J. Mao, Q. Shu, Y. Wen, H. Yuan, D. Xiao, M.M. Choi, Cryst. Growth. Des., 9 (2009) 2546-2548.

[28] M. Nagarathinam, J. Chen, J.J. Vittal, Cryst. Growth. Des., 9 (2009) 2457-2463.

[29] X.L. Yu, C.B. Cao, H.S. Zhu, Q.S. Li, C.L. Liu, Q.H. Gong, Adv. Funct. Mater., 17 (2007) 1397-1401.

[30] P. Roy, K. Mondal, S.K. Srivastava, Cryst. Growth. Des., 8 (2008) 1530-1534.

[31] N. Mukherjee, A. Sinha, G.G. Khan, D. Chandra, A. Bhaumik, A. Mondal, Mater. Res. Bull., 46 (2011) 6-11.

[32] S. Sun, X. Song, C. Kong, D. Deng, Z. Yang, CrystEngComm, 14 (2011) 67-70.

[33] Y.-B. Chen, L. Chen, L.-M. Wu, Cryst. Growth. Des, 8 (2008) 2736-2740.

[34] S.K. Maji, N. Mukherjee, A.K. Dutta, D.N. Srivastava, P. Paul, B. Karmakar, A. Mondal, B. Adhikary, Mater. Chem. Phys., 130 (2011) 392-397.

[35] Y. Xie, L. Carbone, C. Nobile, V. Grillo, S. D'Agostino, F. Della Sala, C. Giannini, D. Altamura, C. Oelsner, C. Kryschi, ACS. Nano., 7 (2013) 7352-7369.

[36] J.A. Turner, Science, 285 (1999) 687-689.

[37] D. Mohan, C.U. Pittman Jr, J. Hazard. Mater., 142 (2007) 1-53.

[38] H.-J. Oh, J.-H. Lee, Y.-J. Kim, S.-J. Suh, J.-H. Lee, C.-S. Chi, Appl. Catal. B-Environ., 84 (2008) 142-147.

[39] D. Mohan, C.U. Pittman, J. Hazard. Mater., 142 (2007) 1-53.

[40] Z. Carmen, S. Daniela, ISBN, (2012) 978-953.

[41] B. Manu, S. Chaudhari, Biores. Technol., 82 (2002) 225-231.

[42] R. Vinu, G. Madras, Environ. Sci. Technol., 43 (2008) 473-479.

[43] C. Pearce, J. Lloyd, J. Guthrie, Dyes. Pigments., 58 (2003) 179-196.

[44] G. McMullan, C. Meehan, A. Conneely, N. Kirby, T. Robinson, P. Nigam, I. Banat, R. Marchant, W. Smyth, Appl. Microb. Biotech., 56 (2001) 81-87.

[45] A.K. Sinha, M. Pradhan, S. Sarkar, T. Pal, Environ. Sci. Technol., 47 (2013) 2339-2345.

[46] W. Epolito, Y. Lee, L. Bottomley, S. Pavlostathis, Dyes. Pigments., 67 (2005) 35-46.

[47] R. Koswojo, R.P. Utomo, Y.-H. Ju, A. Ayucitra, F.E. Soetaredjo, J. Sunarso, S. Ismadji, Appl. Clay. Sci., 48 (2010) 81-86.

[48] S. Merouani, O. Hamdaoui, F. Saoudi, M. Chiha, C. Pétrier, J. Hazard. Mater., 175 (2010) 593-599.

[49] O.J. Hao, H. Kim, P.-C. Chiang, Crit. Rev. Environ. Sci. Technol., 30 (2000) 449-505.

[50] S. Ghoreishi, R. Haghighi, Chem. Eng. J., 95 (2003) 163-169.

[51] N.J. Robinson, S.K. Whitehall, J.S. Cavet, Adv. Microb. Physiol., 44 (2001) 183-213.

[52] D. Acemoglu, S. Johnson, J.A. Robinson, in, Natl. Bureau. Eco. Res., 2000.

[53] V. Kumar, L. Wati, P. Nigam, I. Banat, B. Yadav, D. Singh, R. Marchant, Process. Biochem., 33 (1998) 83-88.

[54] B. Hameed, A.M. Din, A. Ahmad, J. Hazard. Mater., 141 (2007) 819-825.

[55] K. Selvi, S. Pattabhi, K. Kadirvelu, Biores. Technol., 80 (2001) 87-89.

[56] V. Kumar, N. Talreja, D. Deva, N. Sankararamakrishnan, A. Sharma, N. Verma, Desalination, 282 (2011) 27-38.

[57] H. Shon, S. Phuntsho, D. Chaudhary, S. Vigneswaran, J. Cho, Drink. Water. Eng. Sci., 6 (2013) 47-53.

[58] Y. Fu, T. Viraraghavan, Biores. Technol., 79 (2001) 251-262.

[59] D. Tryk, A. Fujishima, K. Honda, Electrochim. Acta., 45 (2000) 2363-2376.

[60] A. Kubacka, M. Fernandez-Garcia, G. Colon, Chem. Rev., 112 (2011) 1555-1614.

[61] J. Kundu, D. Pradhan, ACS. Appl. Mater. Interf., 6 (2014) 1823-1834.

[62] M. Basu, A.K. Sinha, M. Pradhan, S. Sarkar, Y. Negishi, T. Pal, Environmental science & technology, 44 (2010) 6313-6318.

[63] L. Isac, L. Andronic, A. Enesca, A. Duta, J. Photoc. Photobiol. A-Chem., 252 (2013) 53-59.

[64] S.K. Bhar, S. Jana, A. Mondal, N. Mukherjee, J. Colloid. Interf. Sci., 393 (2013) 286-290.

[65] A.K. Dutta, S.K. Maji, D.N. Srivastava, A. Mondal, P. Biswas, P. Paul, B. Adhikary, ACS. Appl. Mater. Interf., 4 (2012) 1919-1927.

[66] S. Sohrabnezhad, A. Pourahmad, E. Radaee, J. Hazard. Mater., 170 (2009) 184-190.

[67] G. Panthi, N.A. Barakat, K. Abdelrazek Khalil, A. Yousef, K.-S. Jeon, H.Y. Kim, Ceramics. Intern., 39 (2013) 1469-1476.

[68] A. Pourahmad, S. Sohrabnezhad, J. Alloy. Compd., 484 (2009) 314-316.

[69] Y. Ni, X. Cao, G. Hu, Z. Yang, X. Wei, Y. Chen, J. Xu, Cryst. Growth. Des., 7 (2007) 280-285.

[70] C. Wang, Y. Ao, P. Wang, S. Zhang, J. Qian, J. Hou, Appl. Surf. Sci., 256 (2010) 4125-4128.

[71] M. El-Kemary, H. El-Shamy, J. Photoc. Photobiol. A-Chem., 205 (2009) 151-155.

[72] F. Chen, Y. Cao, D. Jia, Chem. Eng. J., 234 (2013) 223-231.

[73] H.R. Pouretedal, A. Norozi, M.H. Keshavarz, A. Semnani, J. Hazard. Mater., 162 (2009) 674-681.

[74] M. Sharma, T. Jain, S. Singh, O. Pandey, Solar. Energy., 86 (2012) 626-633.

[75] G. Lin, J. Zheng, R. Xu, J. Phys. Chem. C., 112 (2008) 7363-7370.

[76] M. Luo, Y. Liu, J. Hu, J. Li, J. Liu, R.M. Richards, Appl. Catal.B-Environ., 125 (2012) 180-188.

[77] M. Luo, Y. Liu, J. Hu, H. Liu, J. Li, ACS. Appl. Mater. Interf., 4 (2012) 1813-1821.

[78] R.K. Upadhyay, M. Sharma, D.K. Singh, S. Amritphale, N. Chandra, Separat. Purif. Technol., 88 (2012) 39-45.

[79] B. Pant, H.R. Pant, N.A. Barakat, M. Park, T.-H. Han, B.H. Lim, H.-Y. Kim, Ceramics. Intern., 40 (2014) 1553-1559.

[80] J. Cao, B. Xu, H. Lin, B. Luo, S. Chen, Catal. Commun., 26 (2012) 204-208.

[81] F. Chen, Y. Cao, D. Jia, J. Colloid. Interf. Sci., 404 (2013) 110-116.

[82] H. Zhong, G. Yang, H. Song, Q. Liao, H. Cui, P. Shen, C.-X. Wang, J. Phys. Chem. C., 116 (2012) 9319-9326.

[83] A. Nezamzadeh-Ejhieh, S. Moeinirad, Desalination, 273 (2011) 248-257.

[84] A.N. Ejhieh, M. Khorsandi, J. Hazard. Mater., 176 (2010) 629-637.

CHAPTER-2

EXPERIMENTAL AND CHARACTERIZATION

2.1 Chemicals

All chemicals, organic solvents and reagents were purchased from Sigma-Aldrich, Fluka and E. Merck. Organic solvents acetone, dichloromethane, chloroform, alcohols and *n*-hexane were distilled, purified & dried according to reported methods [1]. Potassium thiocyanate (98 % pure), Copper acetate monohydrate (98 % pure), Propionyl chloride (99 % pure), 4-nitroaniline (99 % pure), 3-nitroaniline (99 % pure), 2-chloro-4-nitroaniline (99 % pure), 2-methyl-4-nitroaniline (99 % pure), 2-methoxy-4-nitroaniline (99 % pure), dimethylsulfoxide (99 % pure) were used without further purification.

2.2 Materials and Methods.

Melting point was determined in a capillary tube using Gallen-Kemp (U.K) electrothermal melting point apparatus. Infrared spectrum was recorded on Thermoscientific NICOLET 6700 FTIR between 4000 and 400 cm^{-1}. ^{1}H and ^{13}C NMR spectra were recorded between 0 and 13 ppm and 0 and 210 ppm respectively on Jeol JNM-LA 500 FT-NMR. $Si(CH_3)_4$ was used as internal reference. UV-vis absorption spectra were recorded on Shimadzu 1800 spectrophotometer between 200 and 800 nm. The CuS nanoparticles were characterized with CuKα radiation of 0.154 nm between diffraction angles of 20-80. Samples were prepared by dispersing them in n-Hexane followed by sonication for 10 minutes. HRTEM of samples was conducted with FEI Company's Titan 80–300 CT transmission electron microscope (TEM) by operating it with the acceleration voltage of 300 kV. Moreover, the EDS spectra of samples were also acquired during their conventional transmission electron microscopic (CTEM) investigations. Finally the SAED patterns from various regions of samples were

acquired for the determination of crystal structures. It should be noted that the entire electron micrographs acquired with TEM were recorded on a 4k x 4k charge coupled devices (CCD) camera of model US4000 from Gatan, Inc.

2.3 Synthesis and Characterization of Ligands

A series of five new nitrosubstituted propionyl thioureas were synthesized from the reaction of propionyl chloride and five different nitroanilines, in the presence of potassium thiocyanate (Figure 2.1). In the first step, propionyl chloride was added drop wise to a solution of potassium thiocyanate in dry acetone, in 1:1 ratio, the reaction mixture was kept on stirring for two h. Formation of white precipitates of potassium chloride (formed as a byproduct), indicated the completion of reaction. In the second step, solution of nitroaniline in dry acetone, again taken in 1:1 ratio was added to the reaction mixture and kept on reflux, overnight. The reaction mixture was then poured in ice and stirred for two hours, thiourea settled down as solid precipitates. The precipitates were collected by filtration, washed with distilled water and dried. All thioureas were tested, for their solubility in different solvents and each was kept for crystallization in acetone [2].

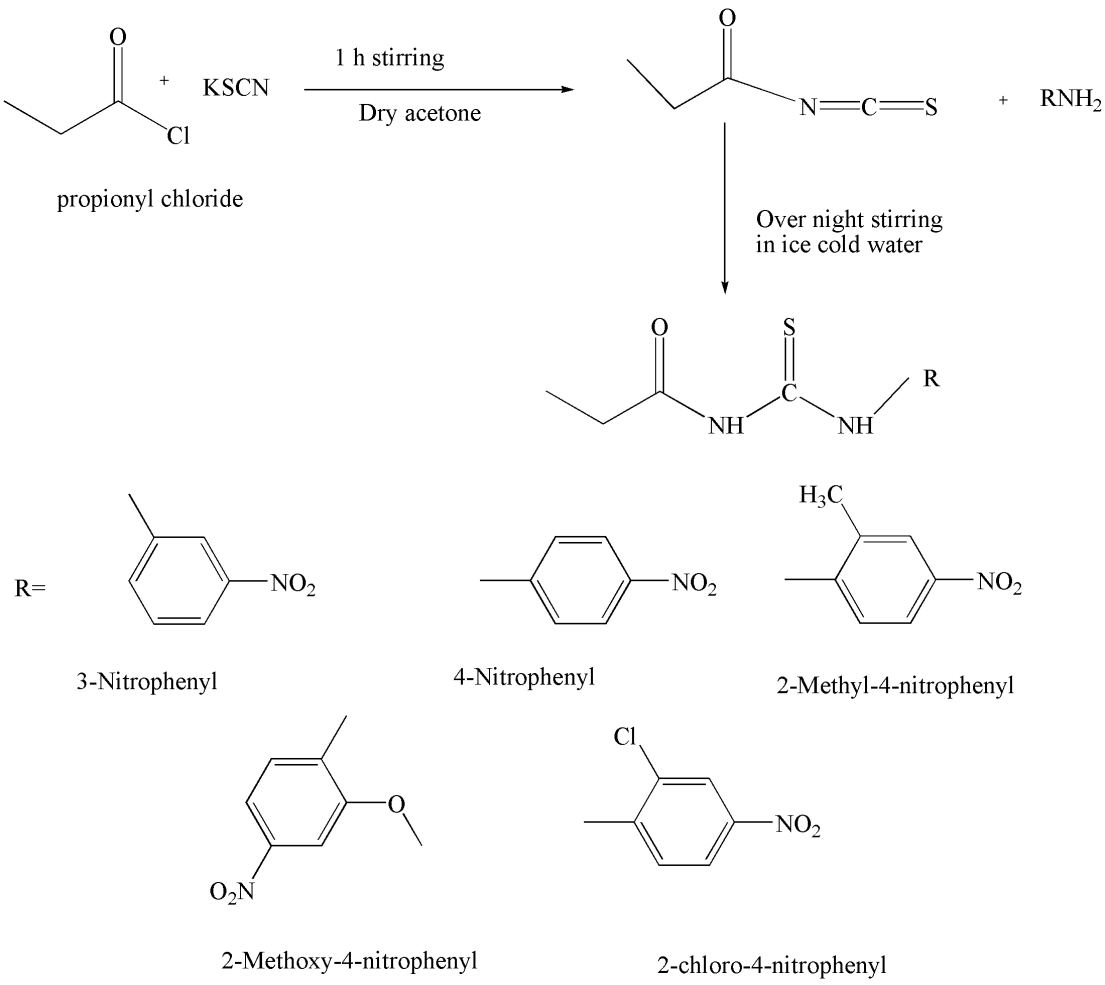

Scheme 1. Synthesis of Ligands

2.3.1 1-(4-nitrophenyl)-3-propionylthiourea (TU1)

Yield (:) 68 %; **mp** 110 °C; **^{1}H NMR (DMSO) δ (ppm)** 12.85 (s, 1H), 11.67 (s, 1H), ~8.2 (dd, *J* = 9.0 Hz, C2H, C6H), ~7.8 (dd, *J* = 9.3 Hz, C3H, C5H) ~2.3 (td, *J* = 44.4 Hz, CH_2), ~1.1 (t, *J* = 15.0, Hz CH_3) ; **^{13}C NMR (DMSO) δ (ppm)** 173.45 (C=O), 181.3 (C=S), 146.00 (C1), 142.3 (C4), 124.7 (C3 & C5), 118.9 (C2 & C6), 30.14 (CH_2), 9.73 (CH_3);. **FTIR υ_{max} (cm^{-1})** 3285 (NH Stretching), 3097 (Ar), 1675 (C=O), 1595 (C-N), 1257 (C=S);

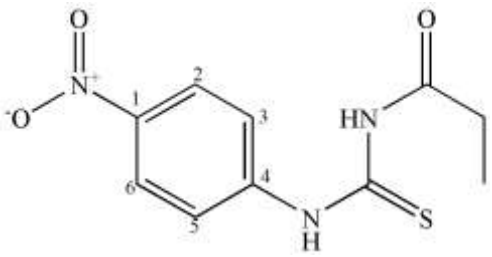

2.3.2 1-(3-nitrophenyl)-3-propionylthiourea (TU2): Yield (:) 73 %; **mp** 106 °C; **H^1 NMR (DMSO) δ (ppm)** 12.65 (s, NH), 11.61 (s, NH), ~8.75 (t, *J* = 4.2 Hz, C2H), ~ 8.10 (td, *J* = 9.0 Hz, C4H), ~7.95 (dd, *J* = 9.0 Hz, C6H), ~7.65 (t, *J* = 16.2 Hz, C5H), 2.4 (dt, *J* = 21.2 Hz, CH2), 1.05 (t, *J* = 14.7 Hz, CH3) (Figure S3) ; **C^{13} NMR (DMSO) δ (ppm)** 179.92 (C=O), 176.59 (C=S), 139.46 (C1), 121.27 (C2), 147.91 (C3), 119.34 (C4), 130.44 (C5), 131.44 (C6), 29.67 (CH_2), 8.97 (CH_3). **FTIR υ_{max} (cm^{-1})** 3283 (NH stretching), 3081 (Ar), 1669 (C=O), 1596 (C-N), 1290 (C=S);

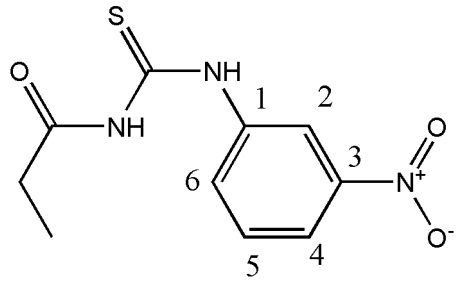

2.3.3 1-(2-chloro-4-nitrophenyl)-3-propionylthiourea (TU3): Yield (:) 73%; **mp** 115 °C; **H^1 NMR (DMSO) δ (ppm)** 12.95 (s, NH), 11.80 (s, NH), ~8.1 (d, *J* = 72.3 Hz, C3H), ~7.9 (dd, *J* = 17.4 Hz, C5H), ~6.8 (t, *J* = 21.9 Hz, C6H), ~2.45 (dd, *J* = 22.5 Hz, CH2), ~1.1 (t, *J* = 15.0 Hz, CH3); **C^{13} NMR (DMSO) δ (ppm)** 176.6 (C=S), 173.73 (C=O) , 141.66 (C1), 136.3 (C2), 125.26 (C3), 143.45 (C4), 116.2 (C5), 127.89 (C6), 29.7 (CH2), 9.76 (CH3). **FTIR υ_{max} (cm^{-1})** 3210 (NH stretching), 3092 (Ar), 1635 (C=O), 1587 (C-N), 1273 (C=S);

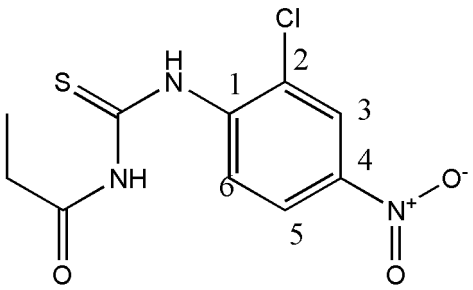

2.3.4 1-(2-methoxy-4-nitrophenyl)-3-propionylthiourea (TU4): Yield (:) 74 %; **mp** 140 °C; **^{1}H NMR (DMSO) δ (ppm)** 13.07 (s, 1H), 11.60 (s, 1H), ~8.1 (d, *J* = 72.3 Hz, C3H), ~7.9 (dd, *J* = 17.4 Hz, C5H), ~6.8 (t, *J* = 21.9 Hz, C6H), 4.02 (s, OCH_3), ~2.4 (q, *J* = 31.9 Hz, CH_2), ~1.07 (t, *J* = 15.0, Hz, CH_3) ; **^{13}C NMR (DMSO) δ (ppm)** 178.4 (C=O), 173.64 (C=S), 155.7 (C2), 140.6 (C4), 128.2 (C1),122.6 (C6), 116.0

(C5), 111.3 (C3), 57.62 (OCH_3), 29.72 (CH_2), 9.96 (CH_3);. **FTIR υ_{max} (cm^{-1})** 3270(NH stretching), 3168 (Ar), 1698 (C=O), 1605 (C-N), 1255 (C=S);

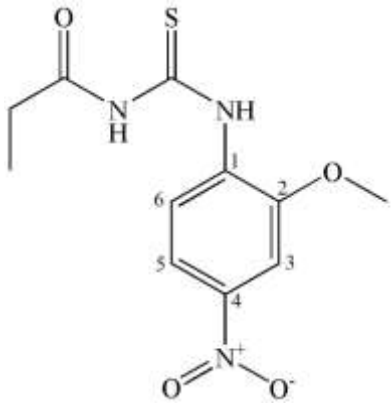

2.3.5 1-(2-methyl-4-nitrophenyl)-3-propionylthiourea (TU5): Yield (:) 71 %; **mp** 131 °C; **^{1}H NMR (DMSO) δ (ppm)** 12.65 (s, 1H), 11.60 (s, 1H), 8.7 (d, *J* = 72.3 Hz, C3H), ~8.3 (dd, *J* = 17.4 Hz, C5H), ~7.9 (t, *J* = 21.9 Hz, C6H), 2.3 (q, 2H), 1.1 (t, 3H) ; **^{13}C NMR (DMSO) δ (ppm)** 179.99 (C=O), 176.76 (C=S), 145.3 (C4), 143.2 (C1), 141.4 (C2), 127.8 (C6), 125.1 (C3), 121.8 (C5), 29.60 (CH_2), 18.8 (C2CH2), 8.94 (CH_3);. **FTIR υ_{max} (cm^{-1})** 3267(NH stretching), 3149 (Ar), 1653 (C=O), 1595 (C-N), 1268 (C=S);

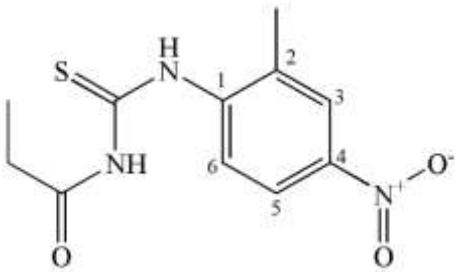

2.4 Synthesis of Complexes

Five new novel nitro substituted copper thiourea (CuTU) complexes were synthesized from the already prepared thioureas (TU). Copper acetate di-hydrate in 20 mL methanol was added drop wise to the solution of TU synthesized in the 1st step in 20 mL of methanol/DCM 1:1 mixture. The solution was then reflux for about 6 h until

formation of green color product. The resulting mixture was then filtered off. Washed several time with methanol and DCM (Scheme 2).

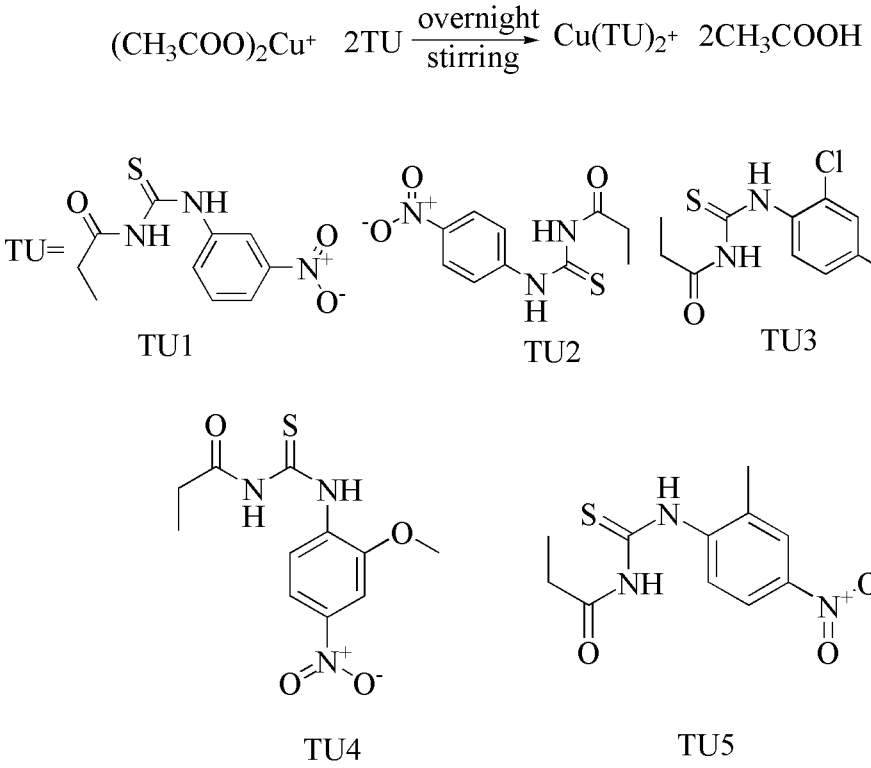

Scheme 2. Synthesis of complexes.

2.4.1 Bis(1-(4-nitrophenyl)-3-propionylthiourea)copper(II) (CuTU1)

Yield (:) 68 %; **mp** 165 °C; **FTIR υ_{max} (cm^{-1})** 3056 (Ar), 1652 (C=O), 1537 (C=N), 1182 (C=S), 444 (CuS);

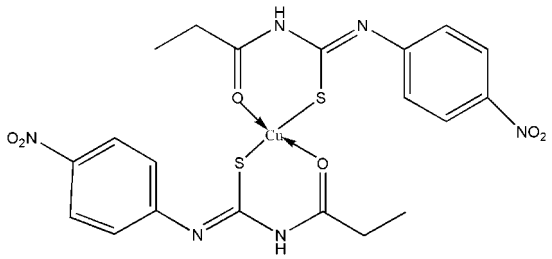

2.4.2 Bis(1-(3-nitrophenyl)-3-propionylthiourea)copper(I) (CuTU2)

Yield (:) 71 %; **mp** 173 °C; **^{1}H NMR (DMSO) δ (ppm)** 10.83 (s, NH), ~8.75 (t, *J* = 44.7 Hz, C2H), ~8.11 (d, *J* = 14.7 Hz, C4H), ~7.8 (dd, *J* = 63.6 Hz, C6H), ~7.3 (d, *J* =

21.0 Hz, C5H), ~2.4 (t, *J* = 36.6 Hz, 2H), 1.04 (s, 3H); **FTIR υ_{max} (cm^{-1})** 3054 (Ar), 1529 (C=N), 1182 (C=S), 436 (CuS);

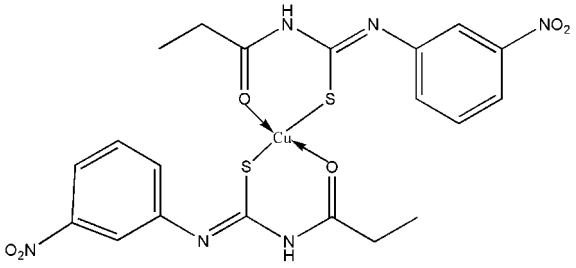

2.4.3 Bis(1-(2-chloro-4-nitrophenyl)-3-propionylthiourea)copper(II) (CuTU3)

Yield (:) 64 %; **mp** 186 °C; **FTIR υ_{max} (cm^{-1})** 3052 (Ar), 1529 (C=N), 1189 (C=S), 432 (CuS);

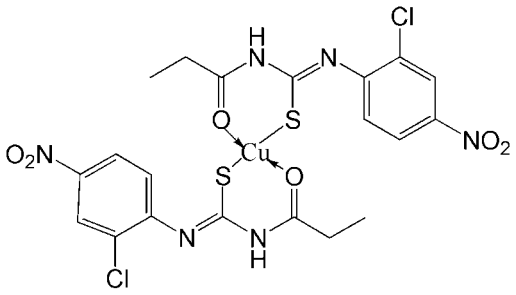

2.4.4 Bis(1-(2-methoxy-4-nitrophenyl)-3-propionylthiourea)copper(II) (CuTU4)

Yield (:) 70 %; **mp** 194 °C; **FTIR υ_{max} (cm^{-1})** 3058 (Ar), 1567 (C=N), 1193 (C=S), 435 (CuS);

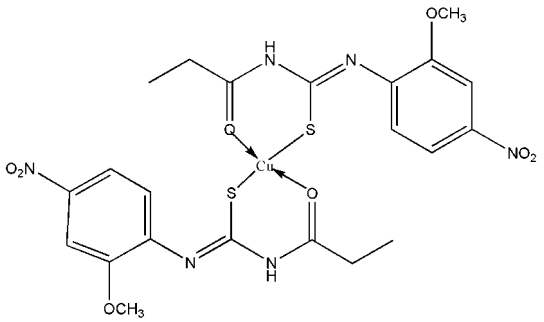

2.4.5 Bis(1-(2-methyl-4-nitrophenyl)-3-propionylthiourea)copper(II) (CuTU5)

Yield (:) 66 %; **mp** 191 °C; **FTIR υ_{max} (cm^{-1})** 3059 (Ar), 1575 (C=N), 1155 (C=S), 443 (CuS);

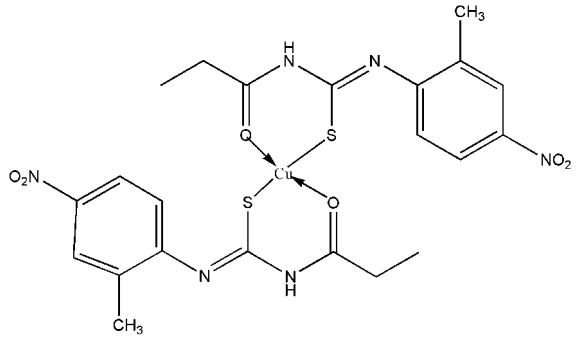

2.5 Fabrication of CuS

CuS nanoparticles and nanorods were then fabricated by using CuTU complexes as a single source precursor under ethylene glycol reducing environment. In case of CuTU1, CuTU2, CuTU3 and CuTU4 only nanoparticles were observed while in case of CuTU5 mixed morphology was observed some i.e. nanorods were surrounded by nanoparticles. 25 mL of ethylene glycol was added to the 0.8 g of CuTU complexes in a two neck round bottom flask. The mixture solution was then reflux for 6-8 h at 180 °C. The resulting solution containing black precipitates was then transferred to a beaker containing methanol to dissolve ethylene glycol and byproducts. The black precipitates were then filtered off, washed several time with deionized water and methanol, and dried in an oven at 70 °C. (Scheme 3).

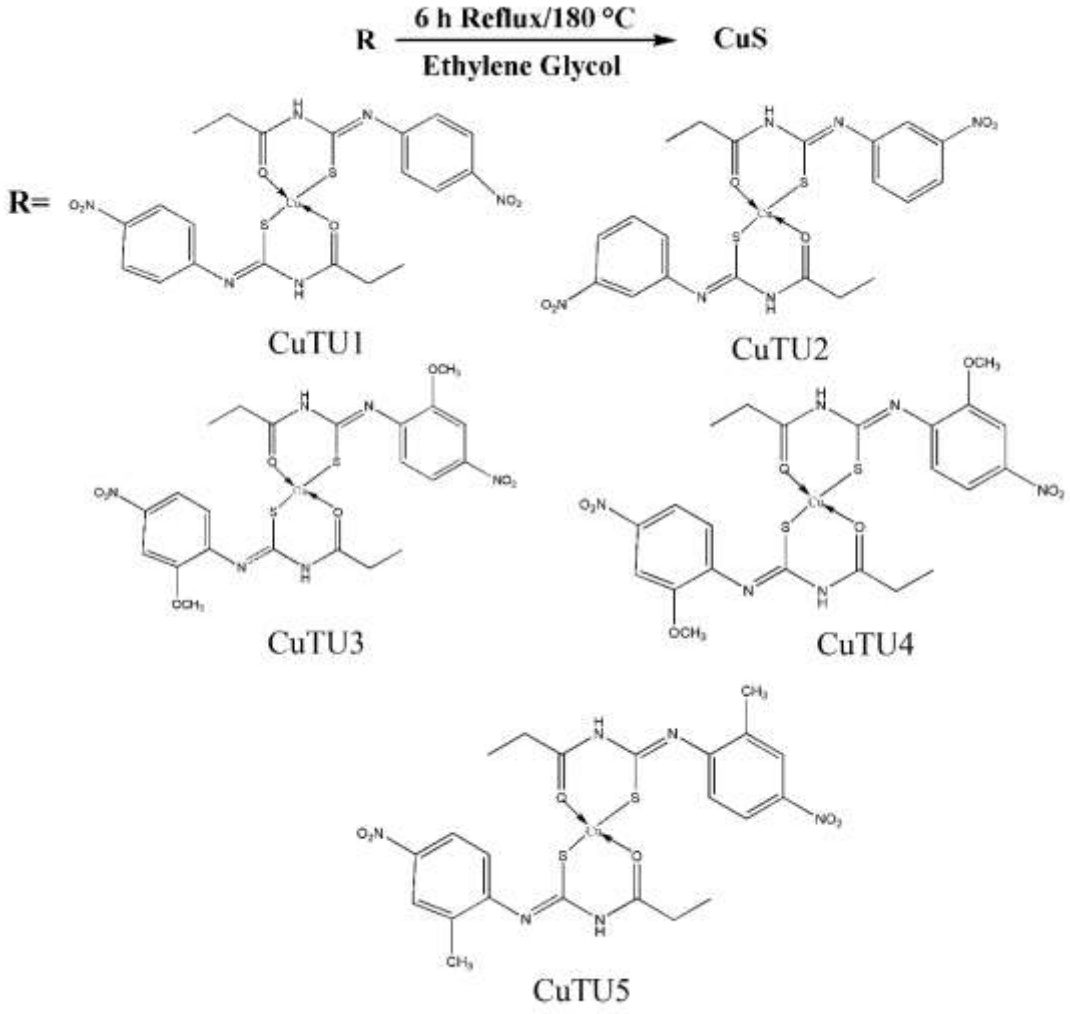

Scheme 3. Fabrication of CuS

2.6 Photocatalytic activity of CuS

The photocatalytic activity was performed considering strong absorption in the visible region and stability of organic dyes under various pH conditions such as cationic dyes methylene blue (MB), malachite green (MG), rhodamine B (RhB), methyl violet (MV) and anionic dye like methyl orange (MO) [3-8]. The photocatalysis was performed under outdoor lightening using direct sunlight as a source of light. The photocatalytic activity of CuS was evaluated individually using 25 mL of 10^{-5} M aqueous solution of dye in the presence of 0.01 g (10 mmol) for complete degradation process. For all organic dyes used for photocatalysis the characteristic absorbance peaks

of dyes decreases with time. The outdoor sunlight has been shown to be very effective for photocatalysis. To further evaluate the self-degradation of dyes under the influence of direct sunlight blank samples without catalyst were also run under the same conditions.

2.7 Battery applications

The battery applications were performed for Lithium ion secondary batteries because CuS has been widely used as a high capacity cathode material previously [9]. Because in these batteries capacity of cathode material is much lower as compared to anode material. The electrochemical performance of the synthesized copper sulfide nanoparticles was evaluated by galvanostatic charge-discharge testing against lithium as counter electrode. The working electrodes were made by a slurry coating procedure. The slurry was prepared by sonicating 80 wt % copper sulfide nanoparticles, 10 wt % acetylene black and 10 wt % PVDF (polyvinylidene fluoride) binder in N-methylpyrrolidinone solvent. This slurry was uniformly coated on aluminum foil current collector. The electrodes were dried in vacuum oven at 100 °C for 12 h. 2025 type coin cell was fabricated in argon filled glove box using polyethylene as separator and 1M $LiPF_6$ in ethylene carbonate/dimethyl carbonate (1:1) as electrolyte. The electrochemical discharge/charge tests of the samples were performed at voltage limits of 1.8 −2.6 V versus Li/Li+.

References

[1] J.A. Riddick, W.B. Bunger, T.K. Sakano, J. Am. Chem. Soc. 6 (1986).

[2] M.K. Rauf, A. Badshah, M. Gielen, M. Ebihara, D.d. Vos, S. Ahmed, J. Inorg. Biochem., 103 (2009) 1135-1144.

[3] Z. Cheng, S. Wang, Q. Wang, B. Geng, CrystEngComm, 12 (2010) 144-149.

[4] M. Basu, A.K. Sinha, M. Pradhan, S. Sarkar, Y. Negishi, T. Pal, Environ. Sci. Technol., 44 (2010) 6313-6318.

[5] C. Ratanatawanate, A. Bui, K. Vu, K.J. Balkus Jr, J. Phys. Chem. C., 115 (2011) 6175-6180.

[6] L. Andronic, L. Isac, A. Duta, J. Photoc. Photobiol. A-Chem., 221 (2011) 30-37.

[7] V.K. Gupta, D. Pathania, S. Agarwal, P. Singh, J. Hazard. Mater., 243 (2012) 179-186.

[8] L. Isac, L. Andronic, A. Enesca, A. Duta, J. Photoc. Photobiol. A-Chem., 252 (2013) 53-59.

[9] J.-S. Chung, H.-J. Sohn, J. Power. Sources, 108 (2002) 226-231.

CHAPTER-3
RESULTS AND DISCUSSION

3.1 Characterization of Precursors

The ligands and complexes were purified on the basis of their solubility in common organic solvents. In ^{1}HNMR spectrum three different types of protons were observed for all synthesized thioureas i.e. NH protons, aromatic protons and aliphatic protons. NH protons were observed as two singlets between 11 and 13 ppm. The NH proton which is present between phenyl ring and thionyl is comparatively more desheilded than NH proton present between thionyl and carbonyl. Aromatic protons were present at their respective positions between 7 to 8.5 ppm and aliphatic protons provide a quartet at 2.5 ppm for CH_2 protons and triplet at ~1 ppm for CH_3 protons. In case of CuTU4 an additional singlet at 4.002 ppm was also observed because of the presence of OCH_3 (Figure 3.1). In ^{13}C NMR maximum downfield carbon is the carbon that is attached with sulphur and appears at 179.9 ppm whereas carbonyl carbon appears at 176.5 ppm. Aromatic carbons provide their peak between ~120 and 140 ppm, while aliphatic carbons provide their peaks below 40 ppm. In the ^{13}CNMR spectrum of CuTU4 an additional singlet due to the presence of OCH3 was observed at 57.6 ppm (Figure 3.2). ^{1}HNMR spectra clearly indicates the formation of complex with $Cu(CH_3COO)_2$ with the disappearance of one NH proton at 12.6 ppm, while rest of the protons appear at their respective positions as for ligands (Figure 3.3).

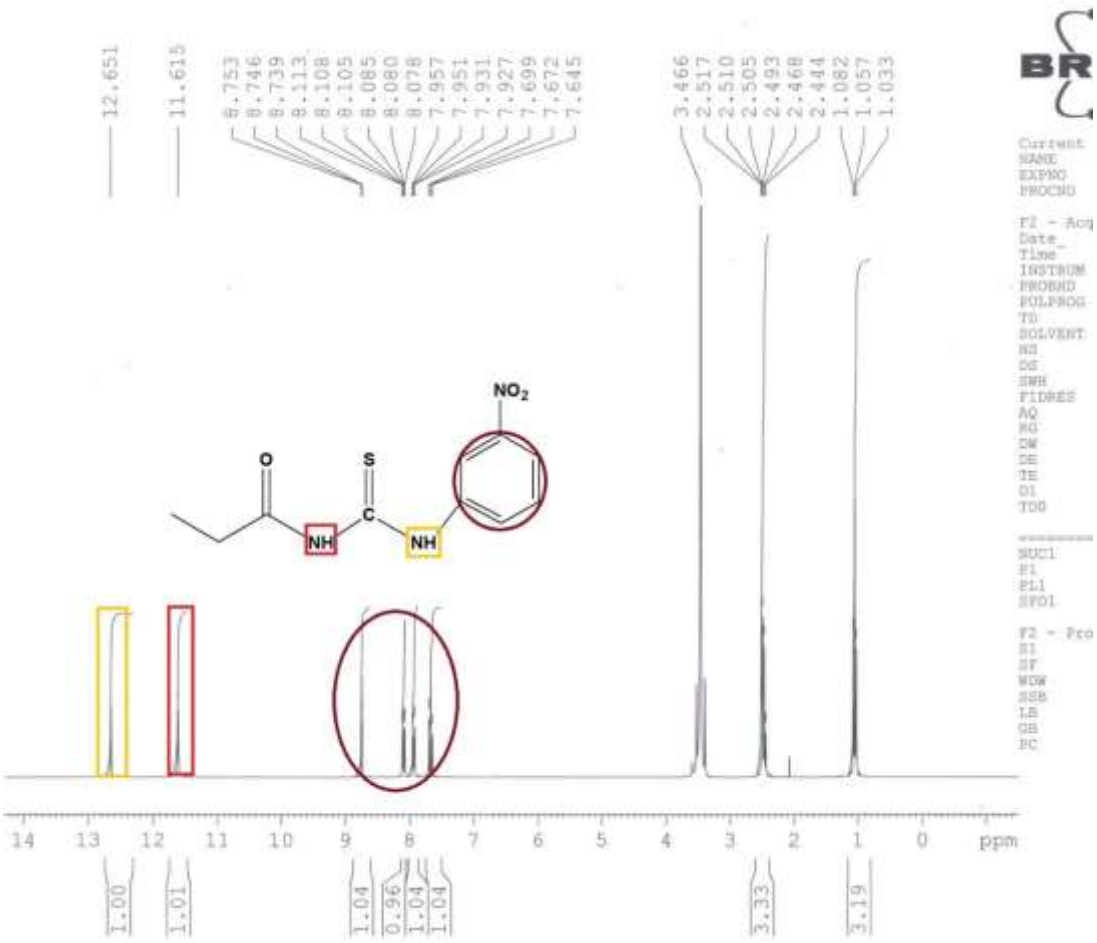

Figure 3.1 [1]HNMR of 1-(3-nitrophenyl)-3-propionylthiourea

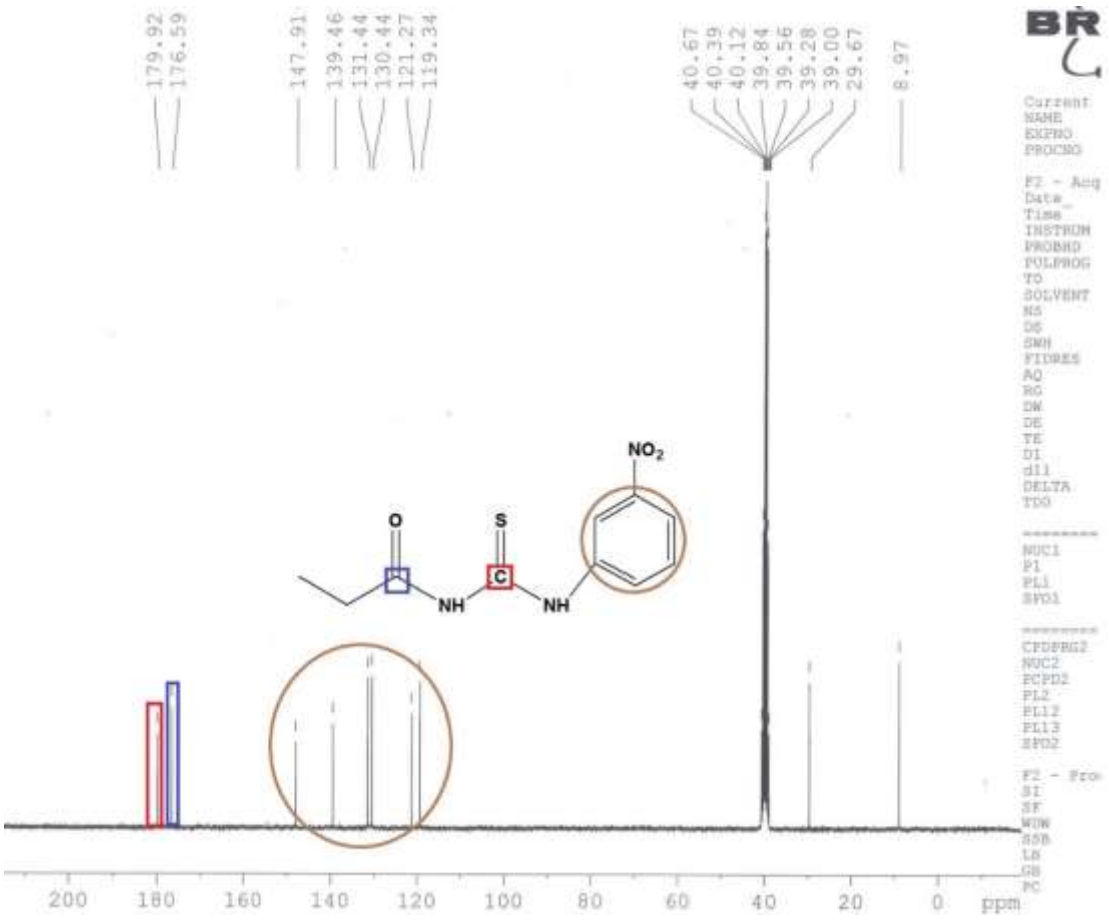

Figure 3.2 ^{13}CNMR of 1-(3-nitrophenyl)-3-propionylthiourea

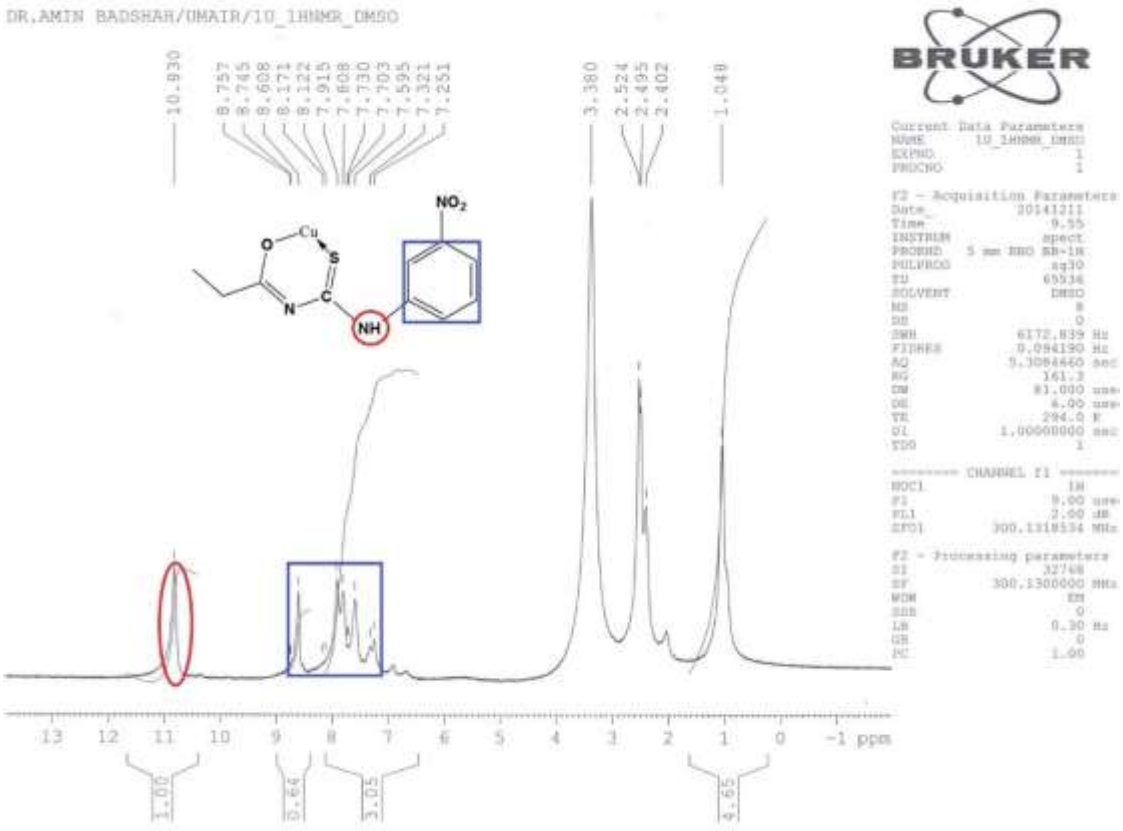

Figure 3.3 [1]HNMR of Bis(1-(3-nitrophenyl)-3-propionylthiourea)copper(I)

In FTIR spectra for ligands NH protons are available between 3200 and 3100 cm^{-1} and Aromatic protons appears slightly above 3000 cm^{-1}. The carbonyl appears above 1650 cm^{-1} as an intense peak while thionyl appears between 1100 and 1300 cm^{-1} (Figure 3. 4). In FTIR spectra the disappearance of NH protons above 3100 cm^{-1} is a strong evidence for complexation between copper and thiourea ligands. The carbonyl peak also shifted to lower frequency and appear as an intense peak between 1530 to 1600 cm^{-1} while thionyl peak appears between 1100 and 1200 cm^{-1}.

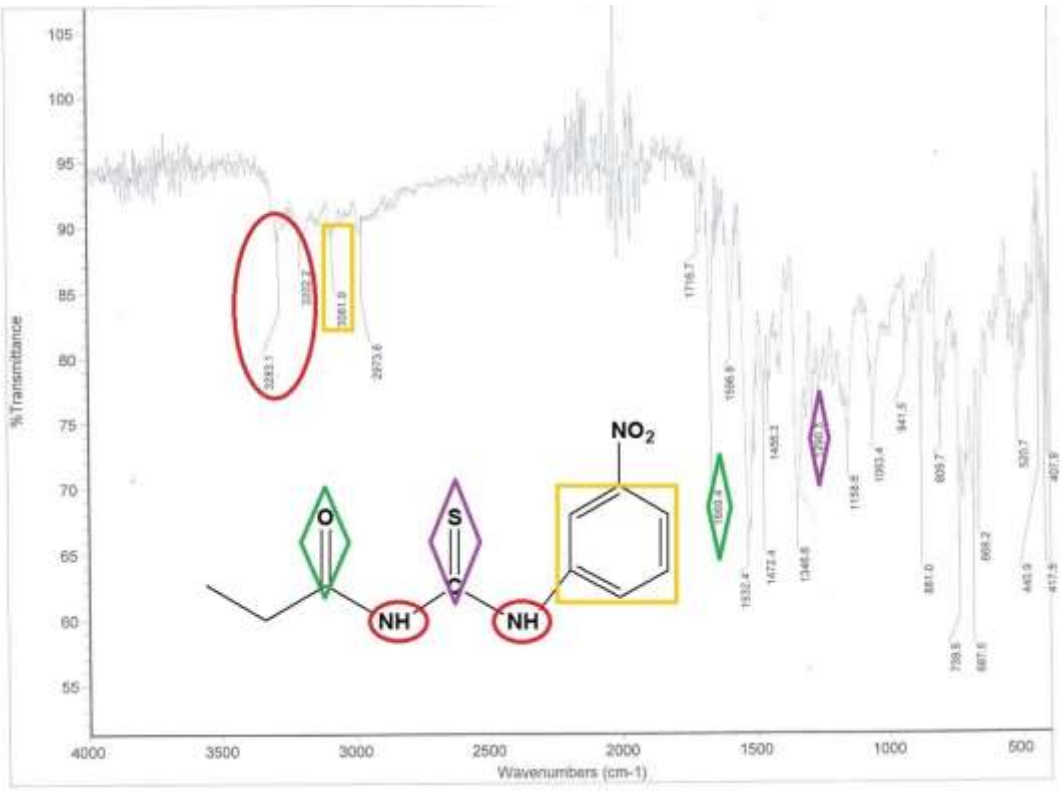

Figure 3.4 FTIR spectrum of 1-(3-nitrophenyl)-3-propionylthiourea

3.2 Characterization of synthesized CuS

Synthesized nanoparticles were characterized using different physical methods available for characterization. Solid CuS can exist in many phases that are stable under normal conditions such as covellite (CuS), anilite ($Cu_{1.75}S$), digenite ($Cu_{1.8}S$), dijuralite ($Cu_{1.96}S$) and chalcocite (Cu_2S) [1]. The purity, phase and polycrystalline nature of the CuS samples are initially characterized using powder X-ray diffraction (PXRD) measurement. The XRD pattern has been compared with the data from JCPDS Card no. 00-001-1281 and indexed as pure hexagonal crystal system of CuS with *P*63/mmc space group and a primitive hexagonal unit cell with $a = 3.8020$ and $c = 16.430$ Å. The presence of strong and sharp diffraction peaks along (101), (102), (103), (110), (108) and (116) planes

indicate the preferential growth of atoms along these plane of primitive hexagonal covellite [2].

3.3 Structural Characterization of CuTU1/CuS

To study the structure and degree of crystallinity of the synthesized CuS nanoparticles HRTEM, EDX and SAED analysis have been performed. The CuS prepared with average of less than 30 nm has been confirmed. The phase purity of CuS has been confirmed by PXRD all the peaks in powder XRD are indexed for hexagonal crystalline phase of Covellite (CuS) with lattices growing mostly in direction of 110 plane. The sharpness of peaks is also an indication of the crystalline nature of the sample (Figure 3.5 a). EDX recorded on nanostructures show the elemental composition of CuS and it is confirmed that sample was enriched with copper and sulphur no additional peaks for other elements were present. Copper CuKα and CuKβ appears at 8.04 and 8.90 KeV which corresponds to X-rays of 1.54 and 1.39 Å and CuLα appears at 0.92 KeV corresponds to emission of 13.33 Å, while SKα appears at 2.37 KeV due to the emission of X-rays in the region of 5.37 Å (Figure 3.5 b). The polynanocrystalline nature of CuS powder is confirmed by SAED images, each cone presents specific planes that were also present in PXRD and confirms d spacing's while cone formation clearly represents the polynanocrystalline nature of the sample (Figure3.5 c). The morphological studies were performed with the help of TEM and interpretation prove that the sample was in the form of well dispersed nanoparticles that are less than 30 nm in size and HRTEM (Figure 3.5 d, e and f) images further confirmed that CuS synthesized were present in the form of nanoparticles and provide lattice fringes for 110 plane having d spacing of 1.89 Å and confirms that most of the particles grow in that specific direction.

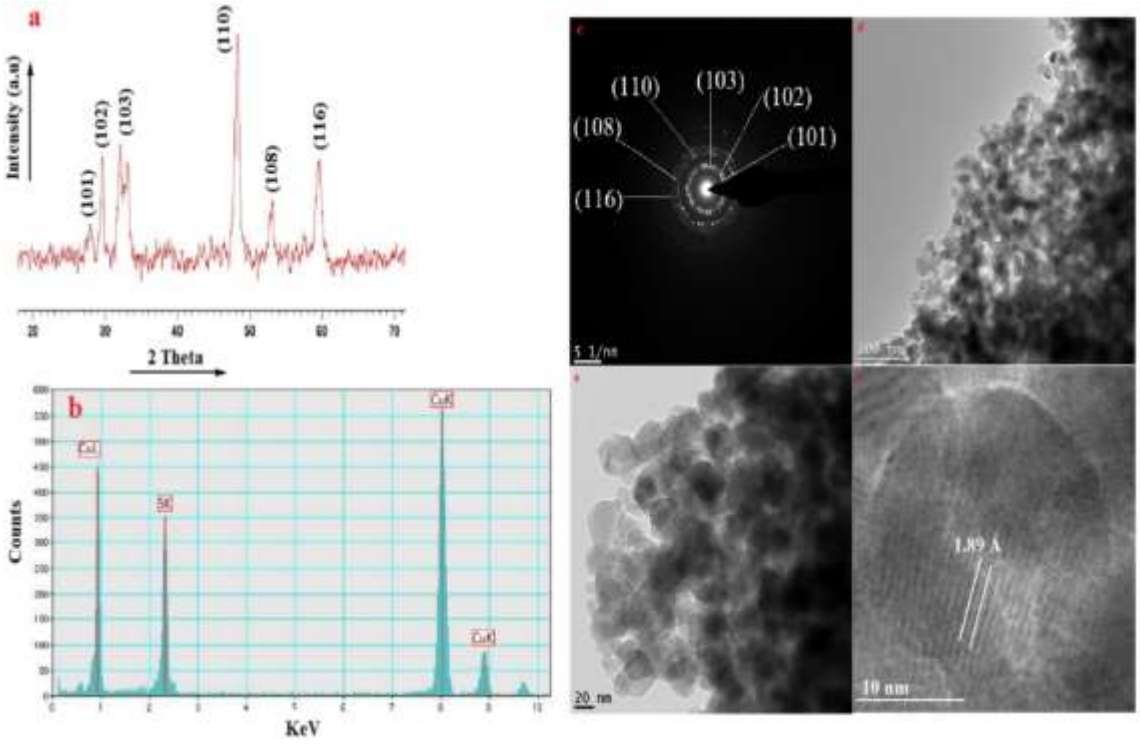

Figure 3.5 a) PXRD **b)** EDX **c)** SAED **d)** TEM image **e and f)** HRTEM image

3.4 Structural Characterization of CuTU2/CuS

To study the structure and degree of crystallinity of the synthesized CuS nanoparticles HRTEM, EDX and SAED analysis have been performed. The CuS prepared with average of less than 30 nm has been confirmed. The phase purity of CuS has been confirmed by PXRD all the peaks in powder XRD are indexed for hexagonal crystalline phase of CuS but in addition to this some other peaks were also appeared in which significant peak at 46.74 2Ɵ is due to the presence of djurleite phase because at high temperature the reduction power of ethylene glycol increases and along with CuS small quantities of djurleite also formed as an impurity (Figure 3.6 a). The EDX recorded on nanostructures show the elemental composition of CuS and it is confirmed that sample was enriched with copper and sulphur (Figure 3.6 b). The polynanocrystalline nature of CuS

powder is confirmed by SAED images (Figure3.6 c). The morphological studies were performed with the help of TEM and HRTEM (Figure 3.6 d, e and f) provide lattice fringes for 110 plane having d spacing of 1.89 Å.

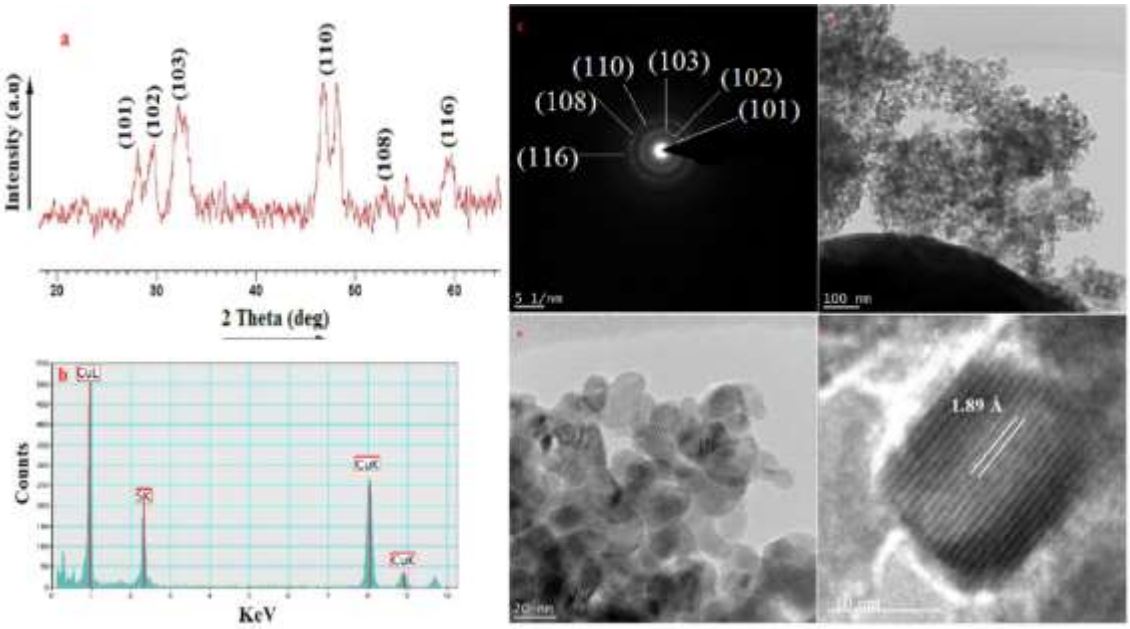

Figure 3.6 a) PXRD **b)** EDX **c)** SAED **d)** TEM image **e and f)** HRTEM image

3.5 Structural Characterization of CuTU3/CuS

To study the structure and degree of crystallinity of the as prepared CuS nanoparticles HRTEM, EDX and SAED analysis have been performed. The CuS prepared with average of less than 30 nm has been confirmed. The phase purity of CuS has been confirmed by PXRD all the peaks in powder XRD are indexed for hexagonal crystalline phase of CuS but in addition to this some other peaks were also appeared in which significant peak at 46.74 2Ɵ is due to the presence of djurleite as an impurity. (Figure 3.7 a). EDX recorded on nanostructures show the elemental composition of CuS and it is confirmed that sample was enriched with copper and sulphur (Figure 3.7 b). The

polynanocrystalline nature of CuS powder is confirmed by SAED images but the cones are not formed in regular fashion which indicates that this sample was slightly less crystalline in nature (Figure3.7 c). The morphological studies were performed with the help of TEM and HRTEM (Figure 3.7 d, e and f) images further confirmed that the CuS synthesized were present in the form of nanoparticles and provide lattice fringes for 110 plane.

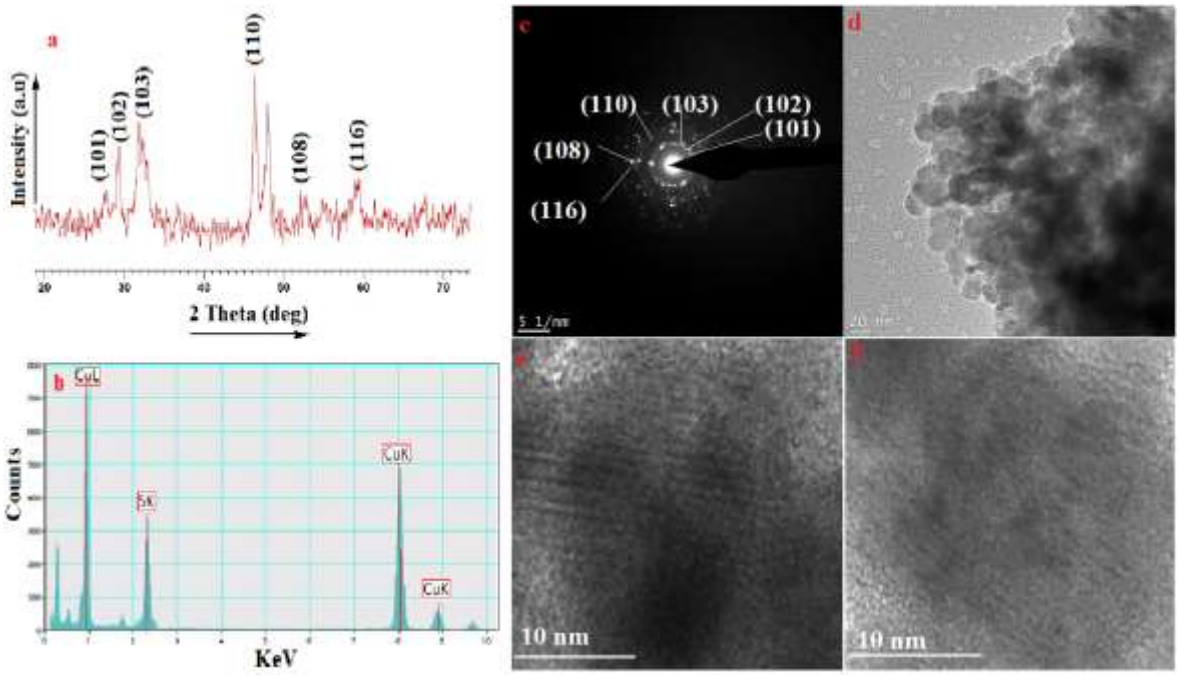

Figure 3.7 a) PXRD **b)** EDX **c)** SAED **d)** TEM image **e and f)** HRTEM image

3.6 Structural Characterization of CuTU4/CuS

To study the structure and degree of crystallinity of the as prepared CuS nanoparticles HRTEM, EDX and SAED analysis have been performed. The CuS prepared with average of less than 30 nm has been confirmed. The phase purity of CuS has been confirmed by PXRD (Figure 3.8 a). EDX recorded on nanostructures show the elemental composition of CuS (Figure 3.8 b). The polynanocrystalline nature of as prepared CuS

powder is confirmed by SAED images (Figure3.8 c). The morphological studies were performed with the help of TEM and HRTEM (Figure 3.8 d, e and f)

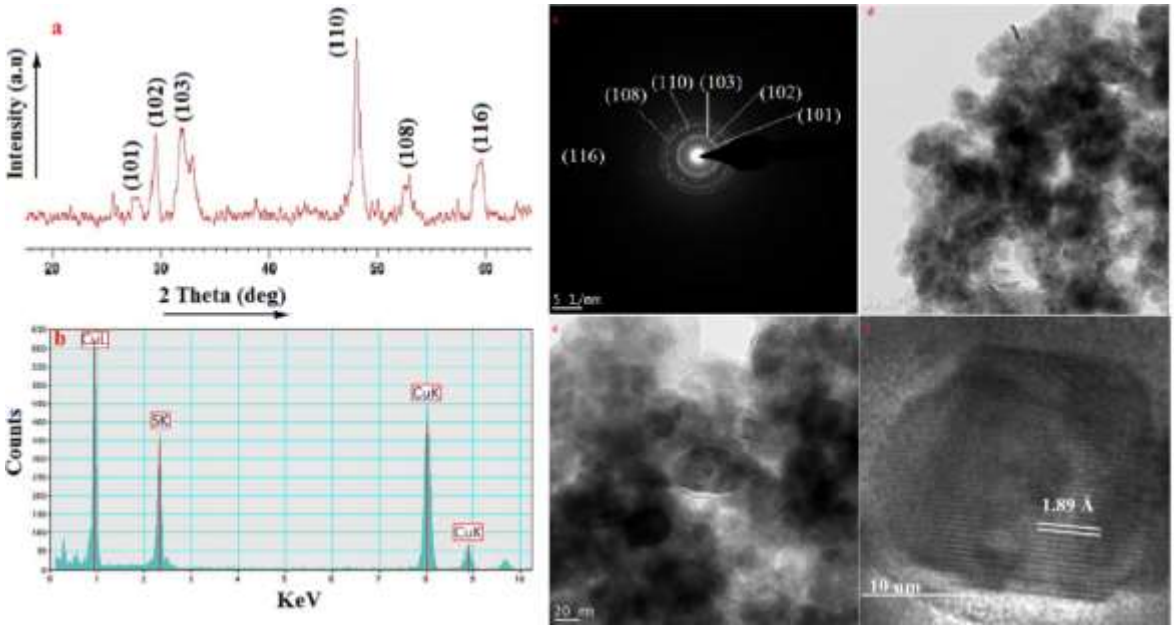

Figure 3.8 a) PXRD **b)** EDX **c)** SAED **d)** TEM image **e and f)** HRTEM image

3.7 Structural Characterization of CuTU5/CuS

To study the structure and degree of crystallinity of the as prepared CuS nanoparticles HRTEM, EDX and SAED analysis have been performed. The CuS prepared with average of less than 30 nm has been confirmed. The phase purity of CuS has been confirmed by PXRD (Figure 3.9 a). EDX recorded on nanostructures show the elemental composition of CuS (Figure 3.9 b). The polynanocrystalline nature of as prepared CuS powder is confirmed SAED images (Figure3.9 c). The morphological studies were performed with the help of TEM and interpretation show that this sample was formed with mixed morphologies i.e. some nanorods were surrounded by nanoparticles in uniform

pattern that are less than 30 nm in size and HRTEM (Figure 3.9 d, e and f) provide lattice fringes for 110 plane.

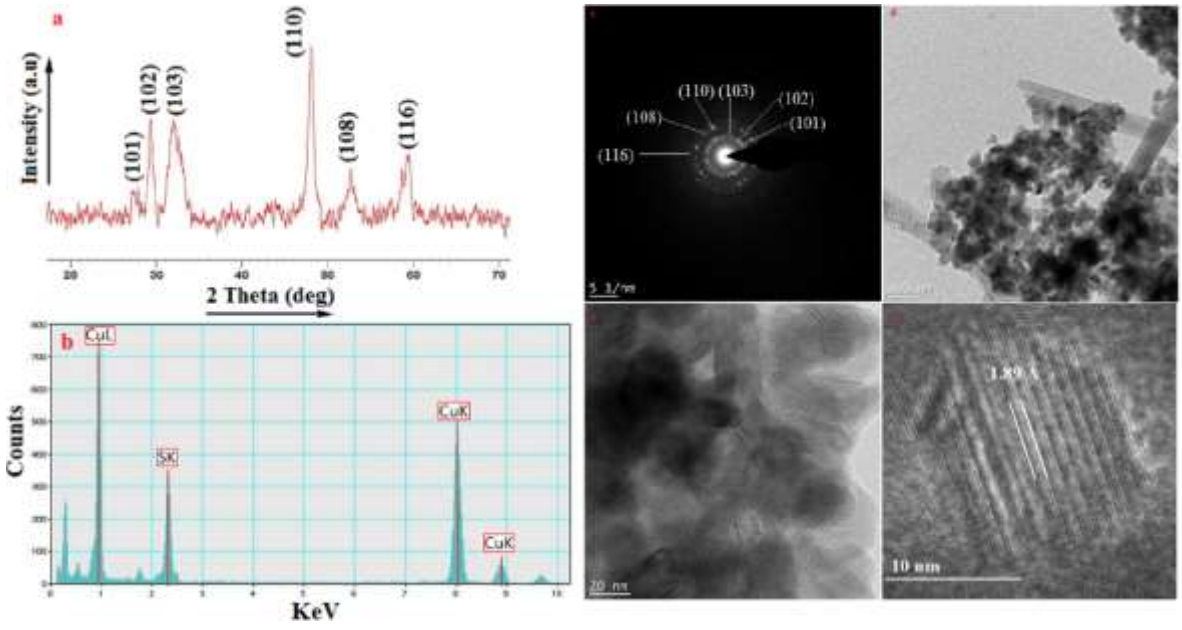

Figure 3.9 a) PXRD **b)** EDX **c)** SAED **d)** TEM image **e and f)** HRTEM image

3.8 Photodegradation of Dye Molecules

Dye degradation depends on the adsorption of dye over catalyst which in turn depends on surface area of catalyst used, the larger the surface area the more is the adsorption. The surface area itself is a dependent quantity which depends on the size of the nanoparticles, the smaller the size larger is the surface area. Keeping these facts in mind CuS were synthesized by using different Cu(TU) complexes as a single source to monitor photocatalytic activities against five different organic dyes.

The average crystallite size which is usually related with the particle size can be derived easily from peak width at different 2Θ values by using Scherrer equation.

$$d = \frac{0.94\,\lambda}{\mathrm{FWHM}(2\theta)\mathrm{Cos}\theta} \qquad \text{Eq no. 3.1}$$

Where d is the diameter of the crystallite site of the nanoparticles and Ɵ is the Bragg's angle of the particular peak under consideration and 0.94 is a constant. The crystallite sizes for CuS made from different precursors are listed in table 3.1

Table 3.1. Crystallite sizes are determined from PXRD peaks

Nanoparticles	**Medium**	**Mean Size (nm)**
CuTU1/CuS	Ethylene glycol	27.5
CuTU2/CuS	Ethylene glycol	15.7
CuTU3/CuS	Ethylene glycol	21.7
CuTU4/CuS	Ethylene glycol	25.0
CuTU5/CuS	Ethylene glycol	16.8

3.9 Photodegradation of Dye Molecules by CuTU1/CuS

The dye solutions in 25 mL volumetric flask containing 10 mg of the catalyst were irradiated under direct sunlight (outdoor lightening) to carryout photodegradation of dyes. The photocatalytic activity of CuS nanoparticles was monitored by successive decrease in the characteristic absorption peaks for different dyes with passage of irradiation time. It was observed that the degradation is quite faster for cationic dyes like methylene blue (MB), rhodamin B (RhB), methyl violet (MV) and malachite green (MG) but quite slow

for anionic dyes like methyl orange (MO). It is quite evident from degradation plots that CuS inherits negative charges on its surface which acts as active agents for degradation of cationic dyes. The negative charge on the surface is possibly due to surface bound OH^-. Electron transfer is facilitated by the electrostatic force of attraction between cationic dye molecules and anionic surface of the catalyst. This is not possible in case of neutral dyes, but in case of large molecules they are flexible and become polarizable due to skeletal spread outs and hence electron transfer is facilitated up to certain extent. Large surface area of catalyst is of prime concern for effective degradation, this is possible in case of nanocatalyst which results in large no of unsaturated coordination sites to adsorb dye molecules. Storage of cationic dyes is also facilitated by the presence of negative sites on the surface of catalyst due to electrostatic force of attraction. The OH^- present on the surface may come from different sources. The possible OH^- sources are: conversion of surface bound oxygen molecules that are adsorbed during the process or through oxidation of water molecules, these water molecules possibly come from the dissociation of ethylene glycol at high temperature. In this way electron transfer in the presence of sunlight is facilitated with reactive oxygen radicles. The two possible oxidative agents that can be consider for the photocatalytic reaction are the photo produced holes and the OH^- radicles that are active degaradation agents [3].

Solar light creates electron holes pairs in the photocatalyst because solar light contain sufficient energy to eject electrons from the photocatalyst that are necessary to react with dissolved oxygen molecules in the sample to form O_2^- and holes then generate OH°. The so formed OH° then act as active center to react with organic dyes to oxidize them (Figure 3.10). To further evaluate the self-degradation of dyes the blank samples were

run under the same conditions without catalyst and it was observed that except malachite green all dyes were quite stable towards direct sunlight hence it can be generalized that electron transfer from catalyst to dyes is facilitated by the generation of electron hole pair under the application of sunlight and in addition to this dye adsorption is necessary for electron transfer otherwise no degradation occurs.

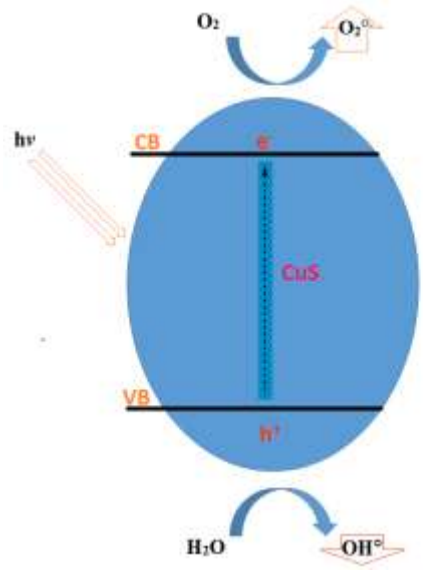

Figure 3.10) Schematic dye degradation by CuS nano-photocatalyst

The characteristic absorption peaks of the dye molecules were used to monitor the degradation of dyes. Successive reduction in peak intensity with time indicates the degradation of dye molecules. Dye degradation was evaluated with the help of following equation.

$$(1-A_t/A_o) \times 100 \qquad \text{Eq. no. 3.2}$$

Where A_o is the initial absorbance and A_t is the absorbance at the time t [4].

In case of methylene blue (MB) the intense peak at 665 nm was used to monitor the overall activity. Almost 60 % degradation was achieved in first 20 minutes, because initially more active centers are available for adsorption of dye molecules while after 180 minutes overall 86 % of the dye degradation was observed (Figure 3.11 a).

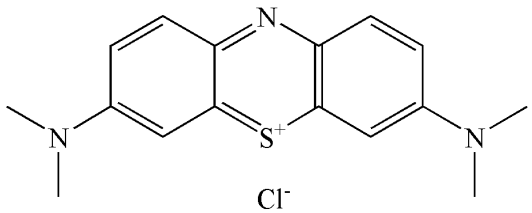

Methylene Blue

In case of malachite green (MG) the peak chosen to observe photocatlytic activity was at 615 nm. It was observed that MG is itself active photochemicaly and degrade under direct sunlight to eliminate itself degradation of MG a blank sample was also run under same conditions without addition of catalyst. After 60 minutes of exposure time dye degraded to 90.31 % with catalyst while without catalyst the degradation was only 61 %. This clearly indicates that the catalyst used was active and degrade dye efficiently (Figure 3.11 b).

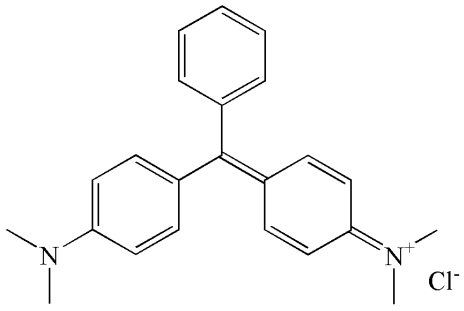

Malachite Green

In case of methyl orang which is an anionic dye the intense peak at 455 nm was used to evaluate the degradation efficiency. Only 5.43 % of dye degradation was observed

with the exposure time of 150 minutes. Further it was observed that in case of methyl orange a blue shift was observed in the characteristic absorption peak in some cases or a shoulder appears with blue shift along with the characteristic absorption peak this is just because of the demethylation of methyl orange and most probably they are replaced with H [5] (Figure 3.11 c).

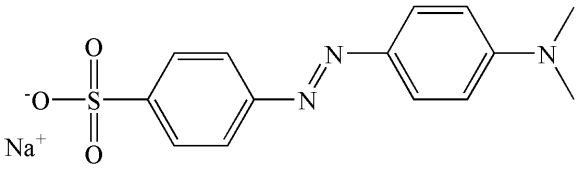

Methyl Orange

Methyl violet (MV) also known as crystal violet bears intense peak at 585 nm that was used to monitor the phtocatalysis. Almost 50 % of degradation was achieved in 10 minutes after exposing under sunlight while 89.49 percent of dye molecules were degraded when samaple was exposed to sunlight for 100 minutes (Figure 3.11 d).

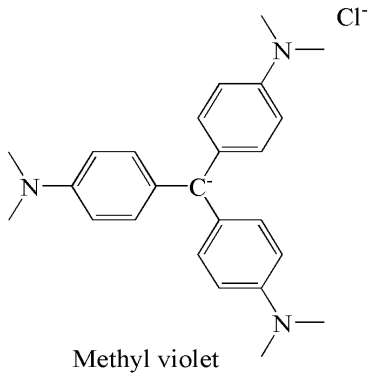

Methyl violet

Rhodamine B (RhB) is another dye that bear active positive nitrogen center and bears intense peak at 525 nm that is the characteristic absorption peak of the dye. 71.36 % of the dye molecules were degraded with the exposure time of 100 minute under direct sunlight (Figure 3.11 e).

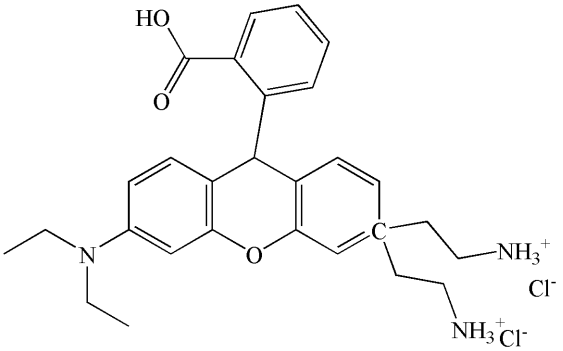

Rhodamine B

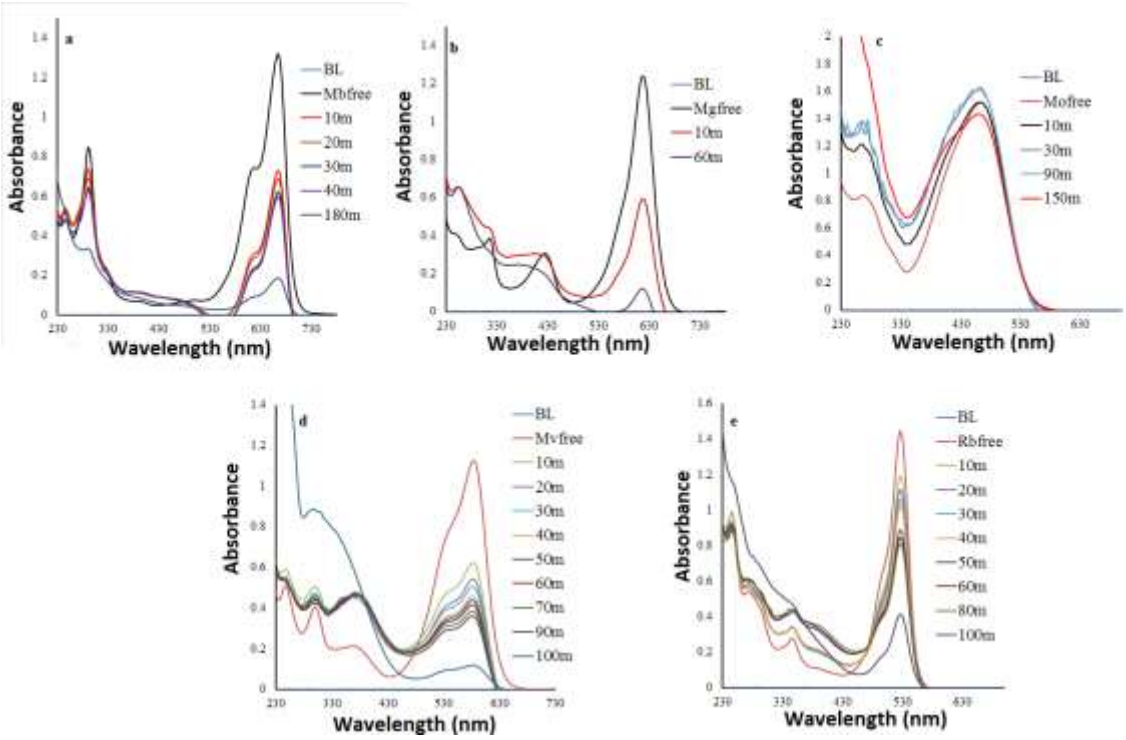

Figure 3.11 UV-visible absorption spectra at different durations with the addition of 10 mg of CuTU1/CuS and irradiated under direct sunlight (outdoor lightening), **a)** Methylene Blue, **b)** Malachite Green, **c)** Methyl Orange, **d)** Methyl Violet, **e)** Rhodamine B.

3.10 Dye Degradation by CuTU2/CuS

Degradation of MB, MG, MO. MV and RhB was estimated to be 81.44%, 93.226%, 13.13%, 84.90% and 87.39% with exposure of 100, 40, 180, 60 and 80 minute at their characteristic peaks (Figure 3.12 a, b, c, d & e).

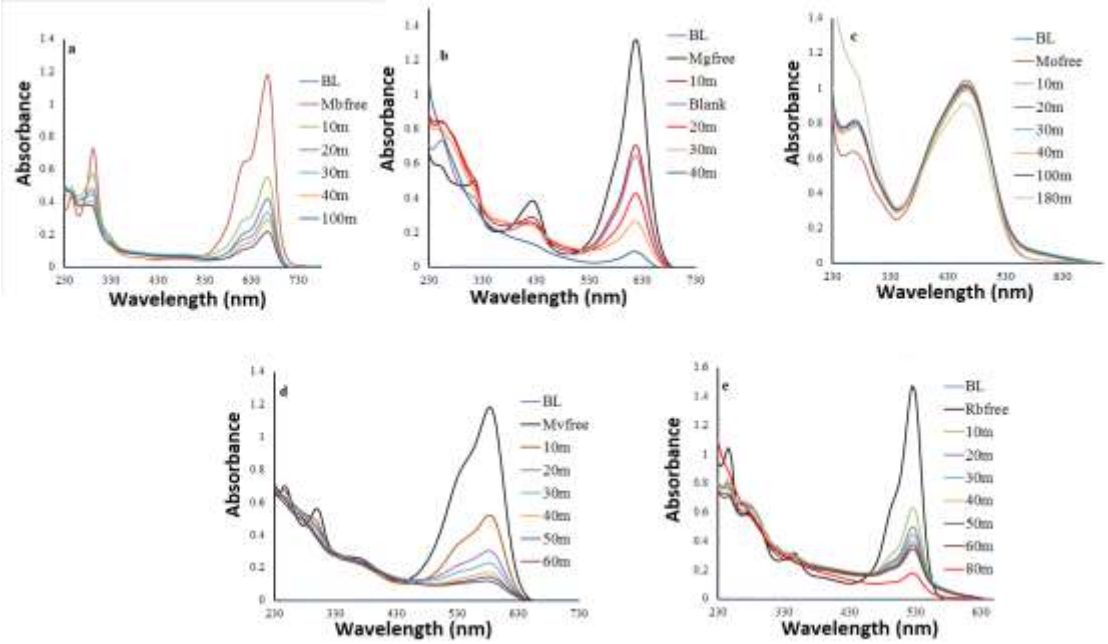

Figure 3.12 UV-visible absorption spectra at different durations with the addition of 10 mg of CuTU2/CuS and irradiated under direct sunlight (outdoor lightening), **a)** Methylene Blue, **b)** Malachite Green, **c)** Methyl Orange, **d)** Methyl Violet, **e)** Rhodamine B.

3.11 Dye Degradation by CuTU3/CuS

Degradation of MB, MG, MO. MV and RhB was estimated to be 61.95%, 90.25%, 9.39%, 85.036% and 70.166% with exposure of 100, 40, 180, 60 and 80 minute at their characteristic peaks. It was also observed that under same conditions the degradation of MV and RhB without catalyst was only 6.143 and 8 % respectively (Figure 3.13 a, b, c, d & e).

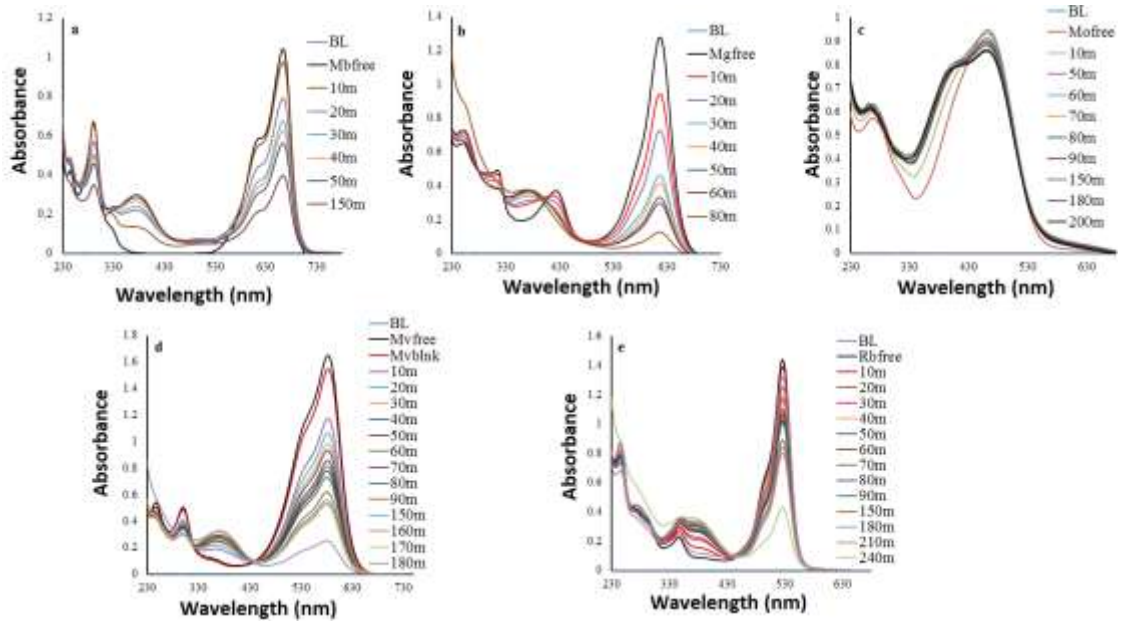

Figure 3.13 UV-visible absorption spectra at different durations with the addition of 10 mg of CuTU3/CuS and irradiated under direct sunlight (outdoor lightening), **a)** Methylene Blue, **b)** Malachite Green, **c)** Methyl Orange, **d)** Methyl Violet, **e)** Rhodamine B.

3.12 Dye Degradation by CuTU4/CuS

Degradation of MB, MG, MO. MV and RhB was estimated to be 79.12%, 77%, 11.15%, 76.89% and 70.28% with exposure of 100, 80, 180, 140 and 160 minute at their characteristic peaks (Figure 3.14 a, b, c, d & e).

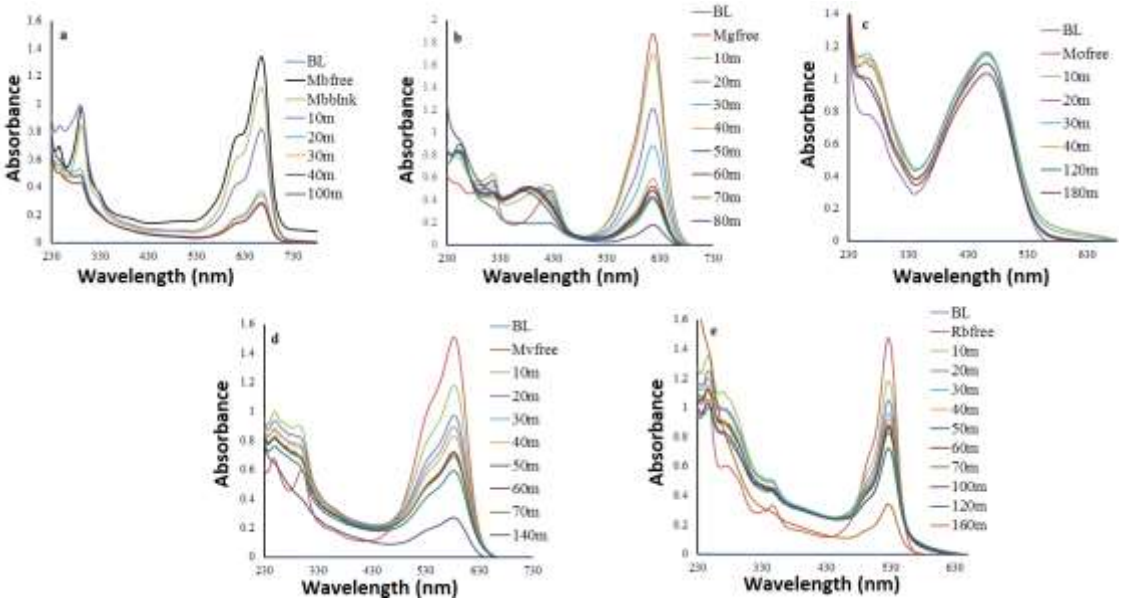

Figure 3.14 UV-visible absorption spectra at different durations with the addition of 10 mg of CuTU4/CuS and irradiated under direct sunlight (outdoor lightening), **a)** Methylene Blue, **b)** Malachite Green, **c)** Methyl Orange, **d)** Methyl Violet, **e)** Rhodamine B.

3.13 Dye degradation by CuTU5/CuS

Degradation of MB, MG, MO. MV and RhB was estimated to be 86%, 90.13%, 5.43%, 89.49% and 79.35% with exposure of 180, 60, 150, 100 and 100 minute at their characteristic peaks (Figure 3.15 a, b, c, d & e).

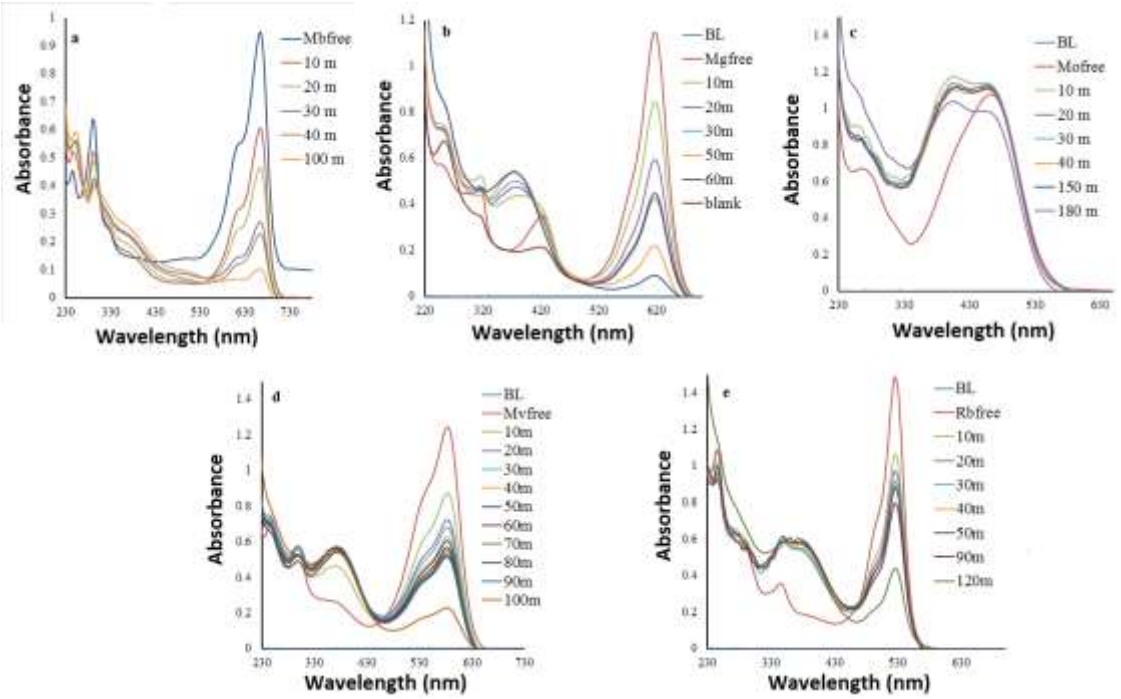

Figure 3.15 UV-visible absorption spectra at different durations with the addition of 10 mg of CuTU5/CuS and irradiated under direct sunlight (outdoor lightening), **a)** Methylene Blue, **b)** Malachite Green, **c)** Methyl Orange, **d)** Methyl Violet, **e)** Rhodamine B.

3.14 Kinetics of Dye Degradation

The dye degradation activity of the CuS was studied by monitoring successive decrease in the characteristic absorption peaks for different dyes. The time dependent relative concentration changes of dyes with CuTU1/CuS (Figure 3.16 a, b, c, d & e), CuTU2/CuS (Figure 3.17 a, b, c, d & e), CuTU3/CuS (Figure 3.18 a, b, c, d & e), CuTU4/CuS (Figure 3.19 a, b, c, d & e) and CuTU5/CuS (Figure 3.20 a, b, c, d & e) are compared. The degradation is considered to be the pseudo first order reaction whose kinetics can be expressed by the equation.

$$A=\text{Ɛ}CL \qquad \text{Eq no. 3.3}$$

$$C=A/\text{Ɛ}L \qquad \text{Eq no. 3.4}$$

Where L is the path length

Ɛ is the molar extinction coefficient that depends on the kind of material used.

$$\ln (C_o/C_t)= kt \qquad \text{Eq no. 3.5}$$

$$k= \ln (C_o/C_t)/t \qquad \text{Eq no. 3.6}$$

Where C_o is the initial concentration of the dye and C_t is the concentration at time "*t*" and *k* is the reaction rate constant [6]. From the given equation reaction rate constants have been investigated and are given in table 3.2.

Dyes	**Ɛ Value**	**References**
MB	76,000 $M^{-1}cm^{-1}$	[7]
MG	147,988 $M^{-1}cm^{-1}$	[8]
MO	24,500 $M^{-1}cm^{-1}$	[9]
MV	362,533 $M^{-1}cm^{-1}$	[10]
RhB	110,000 $M^{-1}cm^{-1}$	[11]

Table 3.2. Comparison of the rate constants for 4NACuS, 3NACuS, 2Cl4NACuS, 2MT4NACuS and 2ME4NACuS

Dyes	Rate constant (min^{-1}) CuTU1/CuS	Rate constant (min^{-1}) CuTU2/CuS	Rate constant (min^{-1}) CuTU3/CuS	Rate constant (min^{-1}) CuTU4/CuS	Rate constant (min^{-1}) CuTU5/CuS
MB	1.00×10^{-2}	1.67×10^{-2}	6.40×10^{-3}	1.54×10^{-2}	2.19×10^{-2}
MG	3.80×10^{-2}	6.72×10^{-2}	2.95×10^{-2}	2.95×10^{-2}	4.20×10^{-2}
MO	3.30×10^{-4}	7.20×10^{-4}	4.93×10^{-4}	6.83×10^{-4}	4.52×10^{-4}
MV	2.20×10^{-2}	3.83×10^{-2}	1.06×10^{-2}	1.07×10^{-2}	1.46×10^{-2}
RhB	1.20×10^{-2}	2.62×10^{-2}	5.0×10^{-2}	9.13×10^{-3}	1.00×10^{-2}

The kinetics for 4 CuTU1/CuS having crystallite size of 27.5 nm shows that degradation is quite faster for malachite green, methyl violet, rhodamine B and methylene blue and slowest for methyl orange. In case of CuTU2/CuS all the rate constants are slightly higher than that for CuTU1/CuS this is just because on decreasing the crystallite size from 27.5 nm to 15.7 nm the surface area is increased and as a result adsorption power of the catalyst increases which in turn facilitate the degradation process. The same trend is repeated with CuTU4/CuS again on increasing the crystallite size from 15.76 nm for 3NACuS to 25 nm for CuTU5/CuS the rate constant decreases but polynanocrystalline nature of the sample remained same in all cases. In case of CuTU3/CuS the average crystallite size decreases to 21.6 nm the expected rate constants should be higher than

CuTU1/CuS and CuTU4/CuS but the trend was not followed as such this is just because of the less crystalline nature of CuTU3/CuS while in case of CuTU5/CuS the same trend follows again. So for degradation process 2 factors must be kept in mind that are operative during the process i.e. the degradation process will be efficient with the decrease in average crystallite size of the catalyst and increases with the increase in crystallinity of the nanoparticles.

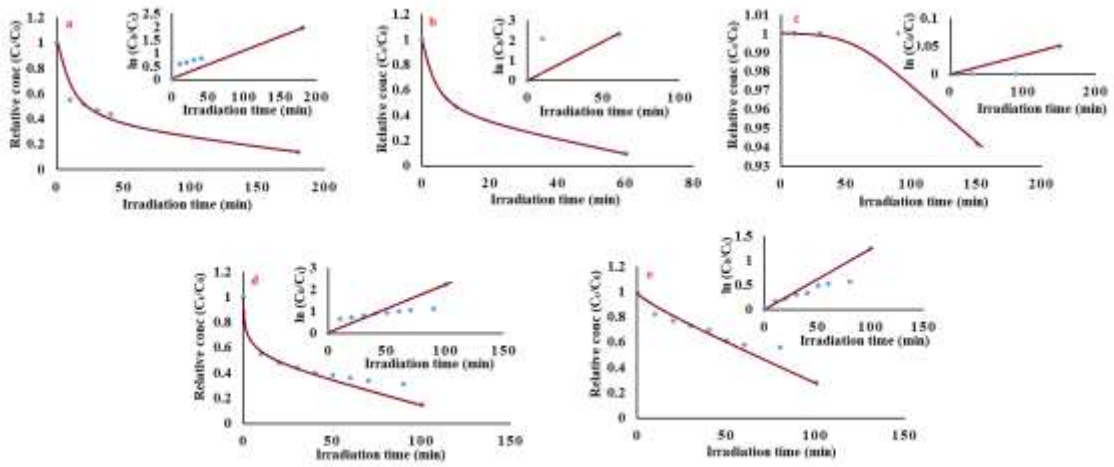

Figure 3.16 Photocatalytic degradation following psuedofirst order kinetics for CuTU1/CuS of **a)** Methylene Blue, **b)** Malachite Green, **c)** Methyl Orange, **d)** Methyl Violet, **e)** Rhodamine B.

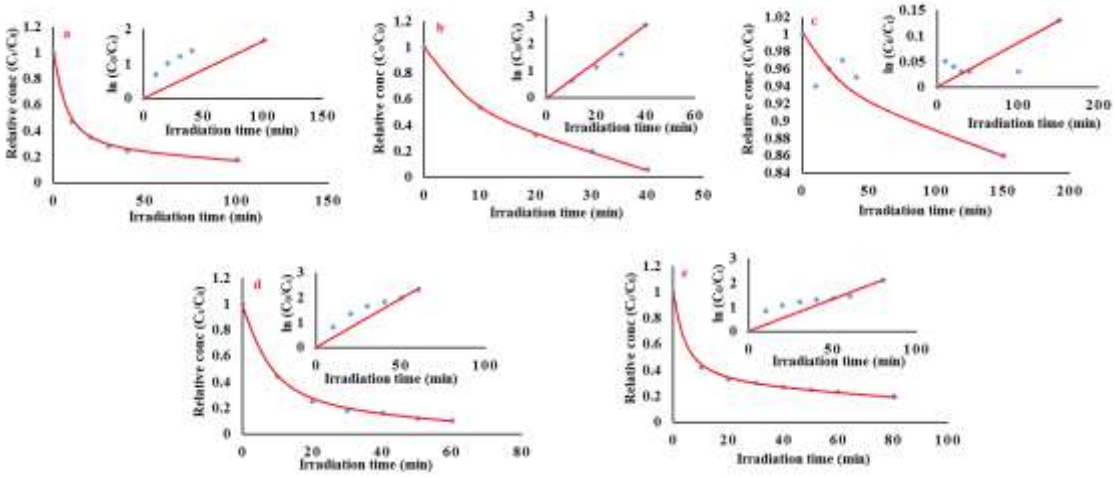

Figure 3.17 Photocatalytic degradation following psuedofirst order kinetics for CuTU2/CuS of **a)** Methylene Blue, **b)** Malachite Green, **c)** Methyl Orange, **d)** MethylViolet, **e)** Rhodamine B.

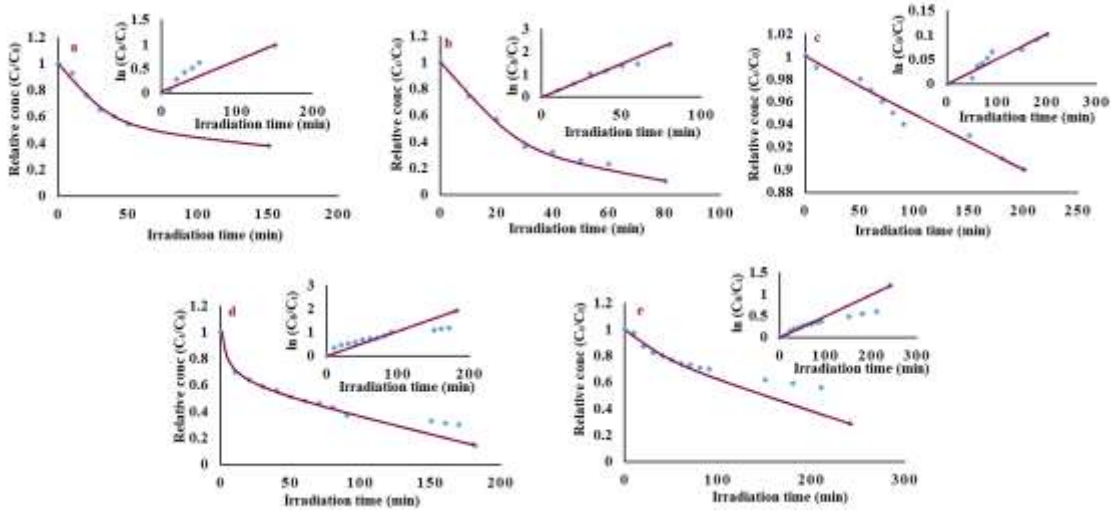

Figure 3.18 Photocatalytic degradation following psuedofirst order kinetics for CuTU3/CuS of **a)** Methylene Blue, **b)** Malachite Green, **c)** Methyl Orange, **d)** Methyl Violet, **e)** Rhodamine B.

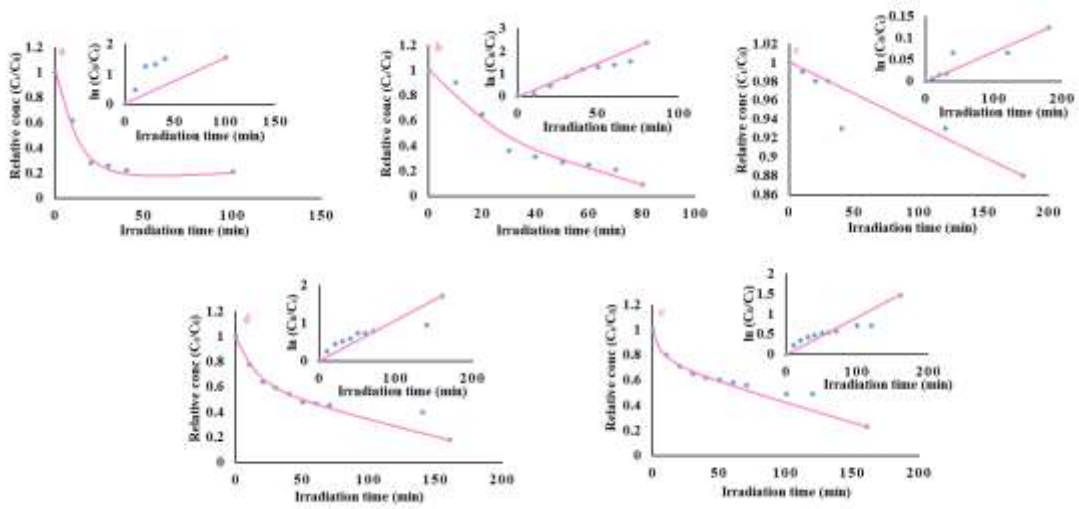

Figure 3.19 Photocatalytic degradation following psuedofirst order kinetics for CuTU4/CuS of **a)** Methylene Blue, **b)** Malachite Green, **c)** Methyl Orange, **d)** Methyl Violet, **e)** Rhodamine B.

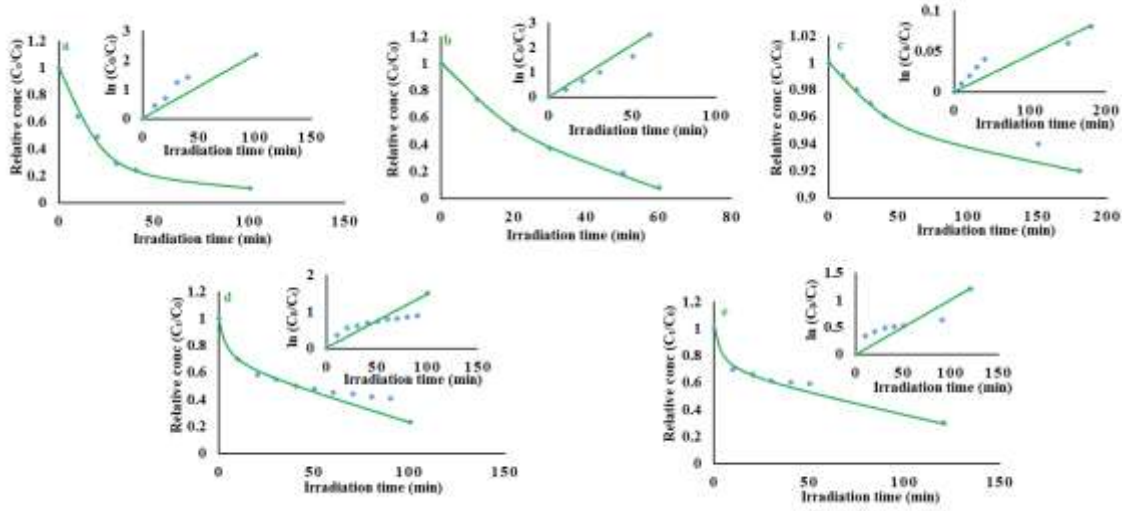

Figure 3.20 Photocatalytic degradation following psuedofirst order kinetics for CuTU5/CuS of **a)** Methylene Blue, **b)** Malachite Green, **c)** Methyl Orange, **d)** Methyl Violet, **e)** Rhodamine B.

3.15 Battery applications

Figure 3.21 shows the typical discharge curves of the copper sulfide electrode at the current density of 100 mAg^{-1} for the first three cycles. The copper sulfide electrode delivers high first cycle specific capacity up to 240 $mAhg^{-1}$. This increased capacity is the result of the nanostructure, high porosity and high surface area of copper sulfide nano particles. This discharge reaction results in the formation of Li_2S and Cu_2S nanoparticles, which results in the loss of first cycle capacity. In the 2nd cycle onward the capacity values are decreased but at lower rate than the initial fading which results in some cycle life stability. Higher discharge capacity can be obtained if we continue the discharge beyond 1.8 V, where a second discharge plateau can be utilized as the result of conversion of Cu_2S to Cu. This results in the permanent failure of the cell, so discharge was limited to 1.8 V cutoff voltage.

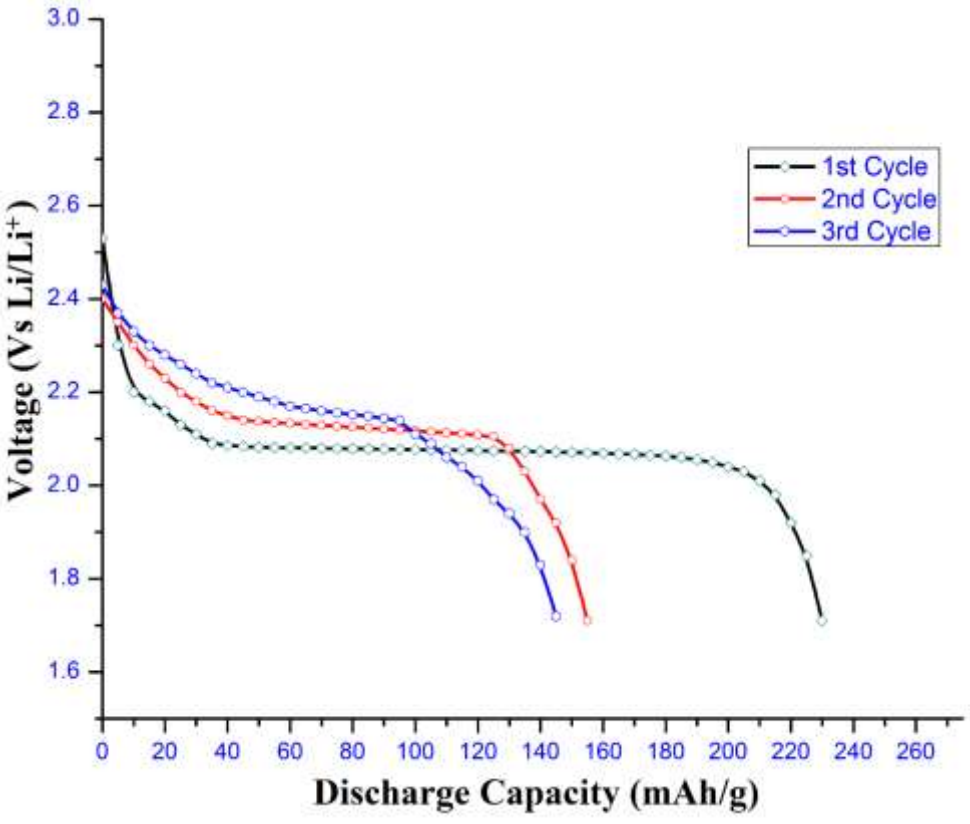

Figure 3.21: Discharge curve of the copper nanoparticles electrode vs Li/Li^+

Figure 3.22 shows the cycling performance of the copper sulfide nanoparticles at a current density of 0.1 Ag^{-1}. It can be clearly seen that after the initial large capacity fading, the fading rate is decreased and material shows stable cycling performance in first 20 cycles.

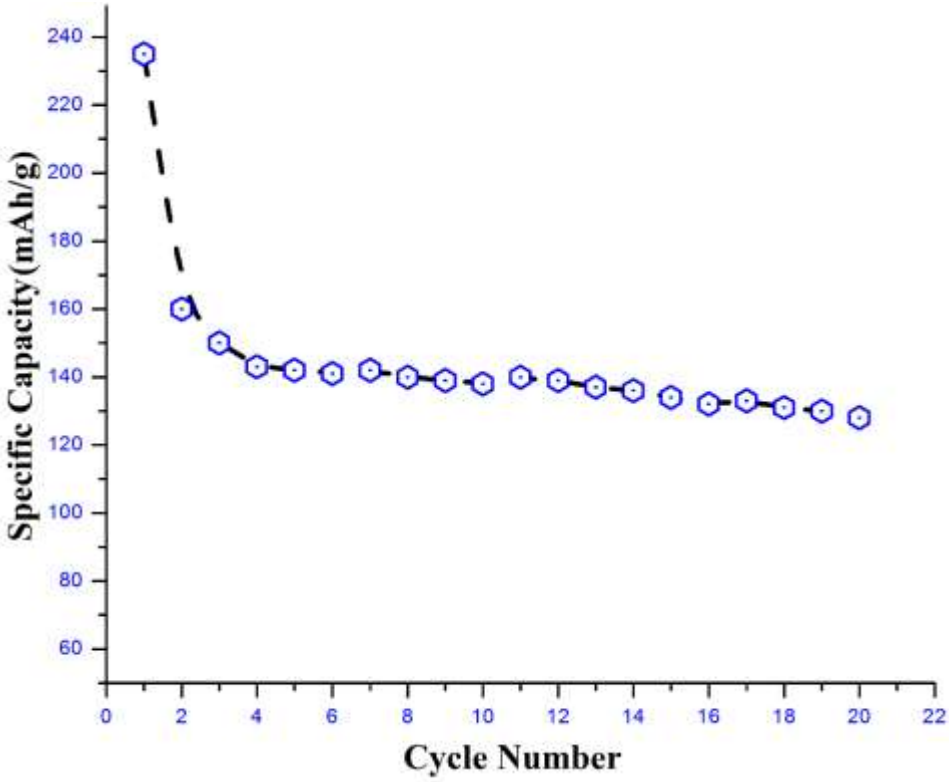

Figure 3.22: Cycling stability of copper sulfide nanoparticles electrode at 0.1C discharge rate

Figure 3.23 shows the rate capability of the copper sulfide electrode. The material is stable at 0.1 C and 0.2 C discharge rates. At 0.5 C the discharge capacity is decreased to 50% of the initial capacity but remains stable for 5 cycles at this rate. At higher current of 1 C rate the capacity is decreased to 30 $mAhg^{-1}$ and declines rapidly. When the rate is reverted to 0.1 C material restores the stable cycling behavior. The high current

performance of the copper sulfide electrode can be further improved by increasing the ratio of the conducting carbon in the electrode.

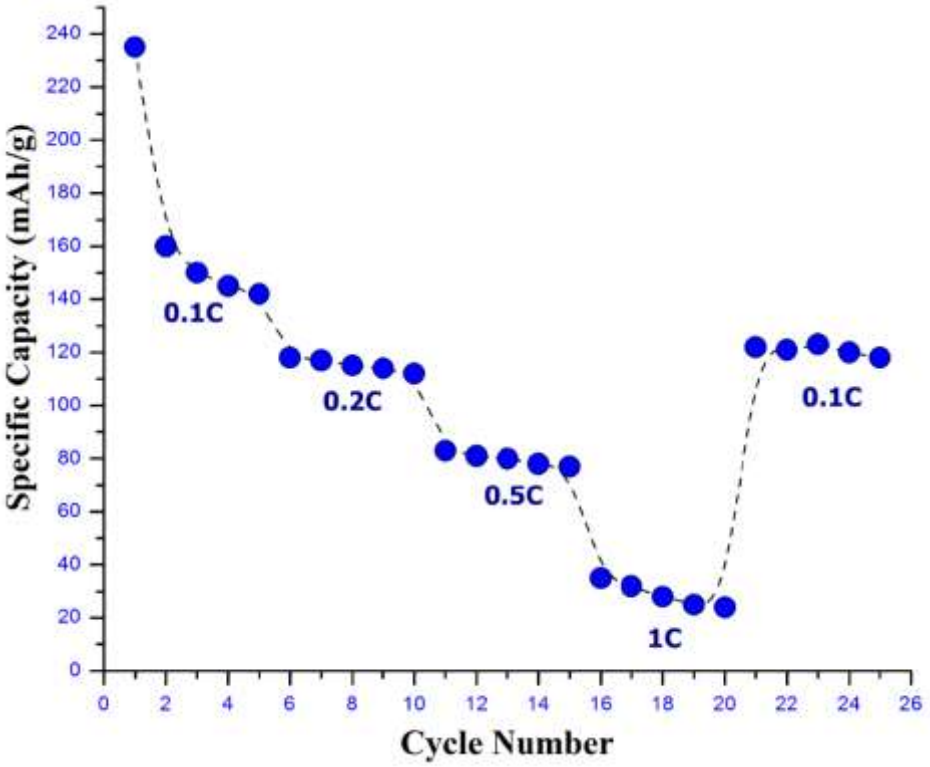

Figure 3.23: Rate capability of the copper sulfide electrode

Conclusion

CuS nanoparticles have been successfully synthesized by using different novel copper thiourea complexes. All of these have been characterized by PXRD, TEM, HRTEM, EDX and SAED. Photocatalytic activity is successfully performed under direct sunlight (outdoor lightening) against five different dyes. The nanomaterial shows high degradation efficiency for cationic dyes but negligible efficiency against anionic dyes. Battery applications are evaluated for 3NACuS by testing electrochemical discharge/charge at voltage limits of 1.8 −2.6 V versus Li/Li+.

References

[1] Y.-B. Chen, L. Chen, L.-M. Wu, Cryst. Growth. Des., 8 (2008) 2736-2740.

[2] Y. Zhu, X. Guo, J. Jin, Y. Shen, X. Guo, W. Ding, J. Mater. Sci., 42 (2007) 1042-1045.

[3] M. Basu, A.K. Sinha, M. Pradhan, S. Sarkar, Y. Negishi, T. Pal, Environ. Sci. Technol., 44 (2010) 6313-6318.

[4] G. Lin, J. Zheng, R. Xu, J. Phys. Chem. C., 112 (2008) 7363-7370.

[5] F.-b. Li, o.-b. Gu, G.-f. Huang, Y.-l. Gu, H.-f. Wan, J. Environ. Sci., 13 (2001) 64-68.

[6] A.K. Dutta, S.K. Maji, D.N. Srivastava, A. Mondal, P. Biswas, P. Paul, B. Adhikary, ACS. Appl. Mater. Interf., 4 (2012) 1919-1927.

[7] M. Hossain, A. Kabir, G. Suresh Kumar, Dyes. Pigments., 92 (2012) 1376-1383.

[8] O. Soriyan, O. Owoyomi, A. Ogunniyi, Acta. Chim. Slov., 55 (2008) 613-616.

[9] K.M. Tawarah, H.M. Abu-Shamleh, Dyes. Pigments., 16 (1991) 241-251.

[10] A. Gupta, A. Pal, C. Sahoo, Dyes. Pigments., 69 (2006) 224-232.

[11] N. Mchedlov-Petrossyan, S. Shapovalov, S. Egorova, V. Kleshchevnikova, E. Arias Cordova, Dyes. Pigments., 28 (1995) 7-18.